RSC Advances

PAPER

View Article Online
View Journal | View Issue

Cite this: *RSC Adv.*, 2021, **11**, 23310

Anticancer activity of pyrimidodiazepines based on 2-chloro-4-anilinoquinazoline: synthesis, DNA binding and molecular docking†

Viviana Cuartas,[ab] Alberto Aragón-Muriel,[c] Yamil Liscano,[d] Dorian Polo-Cerón,[c] Maria del Pilar Crespo-Ortiz,[e] Jairo Quiroga,[a] Rodrigo Abonia[a] and Braulio Insuasty *[ab]

Multidrug resistance to chemotherapy is a critical health problem associated with mutation of the therapeutic target. Therefore, the development of anticancer agents remains a challenge to overcome cancer cell resistance. Herein, a new series of quinazoline-based pyrimidodiazepines **16a–g** were synthesized by the cyclocondensation reaction of 2-chloro-4-anilinoquinazoline-chalcones **14a–g** with 2,4,5,6-tetraaminopyrimidine. All quinazoline derivatives **14a–g** and **16a–g** were selected by the U.S. National Cancer Institute (NCI) for testing their anticancer activity against 60 cancer cell lines of different panels of human tumors. Among the tested compounds, quinazoline-chalcone **14g** displayed high antiproliferative activity with GI_{50} values between 0.622–1.81 μM against K-562 (leukemia), RPMI-8226 (leukemia), HCT-116 (colon cancer) LOX IMVI (melanoma), and MCF7 (breast cancer) cancer cell lines. Additionally, the pyrimidodiazepines **16a** and **16c** exhibited high cytostatic (TGI) and cytotoxic activity (LC_{50}), where **16c** showed high cytotoxic activity, which was 10.0-fold higher than the standard anticancer agent adriamycin/doxorubicin against ten cancer cell lines. COMPARE analysis revealed that **16c** may possess a mechanism of action through DNA binding that is similar to that of CCNU (lomustine). DNA binding studies indicated that **14g** and **16c** interact with the calf thymus DNA by intercalation and groove binding, respectively. Compounds **14g**, **16c** and **16a** displayed strong binding affinities to DNA, EGFR and VEGFR-2 receptors. None of the active compounds showed cytotoxicity against human red blood cells.

Received 5th May 2021
Accepted 25th June 2021

DOI: 10.1039/d1ra03509f

rsc.li/rsc-advances

1. Introduction

Cancer is a life-threatening disease and the second cause of death globally,[1,2] accounting for 9.6 million deaths in 2018,[3] according to the World Health Organization (WHO), with lung, prostate, colorectal, stomach, liver, breast, cervical, and thyroid being the most common types of cancer.[3] Therefore, the development of anticancer agents remains an important field of research to find alternatives to the chemotherapy toxicities and to overcome the intrinsic cancer cell resistance.[4] Traditional chemotherapy affects the main signaling pathways, cell proliferation, survival, migration, adhesion, differentiation, and overexpression in several solid tumors,[1,5] with the epidermal growth factor receptor (EGFR) being one of the most used therapeutic targets to block progression of different types of malignant tumors,[1] including lung, breast, esophageal, colon, pancreatic and prostate cancer.[6] The first-generation of EGFR tyrosine kinase inhibitors (TKIs) agents gefitinib and erlotinib (Fig. 1) rapidly shrink tumor size in the treatment of non-small cell lung cancer (NSCLC),[6,7] as well as, lapatinib is recognized as a dual EGFR and HER2 (human epidermal growth factor receptor 2) inhibitor, approved for metastatic breast cancer.[5] These tyrosine kinase inhibitors (gefitinib, erlotinib, and lapatinib) are reversible competitors against the binding site of the EGFR, and they have been used with some clinical success.[7] However, the patients develop acquired resistance to gefitinib and erlotinib within 10–16 months of treatment.[7] On the other hand, the second-generation EGFR inhibitors (such as afatinib, canertinib, dacomitinib, Fig. 1) have been developed as irreversible inhibitors against Cys797,[5,8] allowing to overcome EGFR-TK mutation-related resistance in clinical trials. Nevertheless, these chemotherapeutic agents have a limited therapeutic window,[5,7] so the acquired resistance remains a major clinical problem.

[a]*Heterocyclic Compounds Research Group, Department of Chemistry, Universidad del Valle, A.A. 25360 Cali, Colombia. E-mail: braulio.insuasty@correounivalle.edu.co; Fax: +57-2339-3248; Tel: +57-315-484-6665*

[b]*Center for Bioinformatics and Photonics-CIBioFI, A.A. 25360 Cali, Colombia*

[c]*Laboratorio de Investigación en Catálisis y Procesos (LICAP), Departamento de Química, Universidad del Valle, Cali 760001, Colombia*

[d]*Grupo de Investigación en Química y Biotecnología (QUIBIO), Universidad Santiago de Cali, Cali 760035, Colombia*

[e]*Grupo de Biotecnología e Infecciones Bacterianas, Departamento de Microbiología, Universidad del Valle, Cali 760043, Colombia*

† Electronic supplementary information (ESI) available: Table S1, spectra data and Fig. S1. See DOI: 10.1039/d1ra03509f

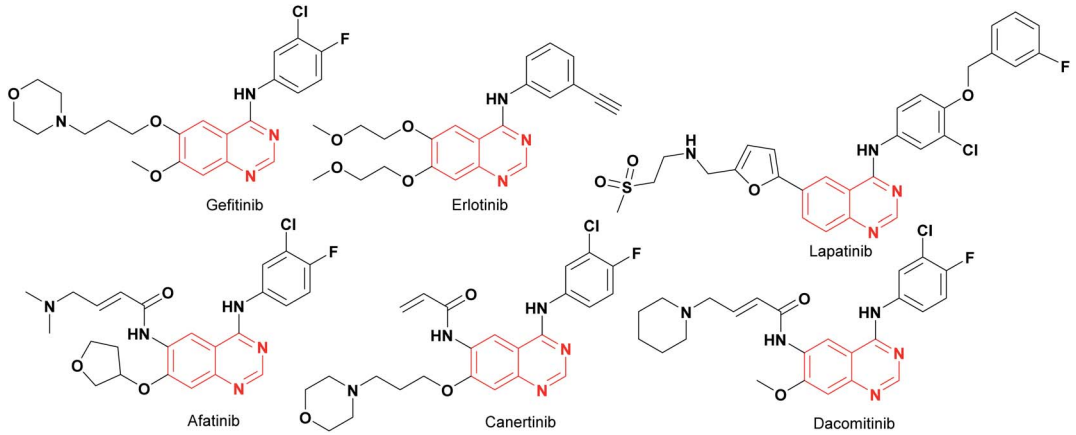

Fig. 1 The first- and second-generation EGFR-TKIs agents.

Recently, computational approaches and rational strategies have allowed the design of ligands directed toward multiple therapeutic targets as an alternative to traditional pharmacological therapy.[9] Although, the main target of 4-anilinoquinazolines is the EGFR,[1,10,11] some derivatives also target several kinases due to the similarities of their binding pockets[6] such as B-Raf, phosphoinositide 3-kinase (PI3K), HER2 and, vascular endothelial growth factor (VEGFR-2), as well as the dual inhibitors afatinib (EGFR/HER2), lapatinib (EGFR/HER2) and vandetanib (EGFR/VEGFR-2).[10] Among recently reported examples, 2-chloro-4-anilinoquinazolines with heterocyclylsulfonamido moiety have shown antitumor activity (**1–2**, Fig. 2), highlighting compound **2**, which displayed an IC_{50} value of 0.13 nM against MCF-7 human breast carcinoma cell line.[12] Barbosa, M. *et al.*[13] designed and synthesized a novel 2-chloro-quinazoline as EGFR and VEGFR-2 dual inhibitor (**3**, Fig. 2), which was approximately 11- and 7-fold more potent on EGFR and VEGFR-2 compared to prototype **2.** In both series including a functional group as hydrogen bond acceptor for binding to the therapeutic target similar to sorafenib and tivozanib (Fig. 2), which form hydrogen bonding interactions between urea fragment with the amino acids **Glu855** and **Asp1046** in VEGFR-2.[6,11,13] In Fig. 2, dual EGFR and VEGFR-2 inhibitors containing the 2-chloro-quinazoline core are shown.[9]

Although, quinazoline derivatives have exhibited high affinity and selectivity as tyrosine kinase inhibitors (TKIs), those compounds can interact with double-stranded DNA due to their planar conjugated system through intercalation and groove binding to DNA[14] with recognition mainly for GC-rich sequences.[15] These types of interactions lead to cell death by disrupting replication and transcription.[14] Therefore, quinazolines represent an important scaffold to the development of DNA-targeted anticancer agents.[14,16]

Pyrimidodiazepines are an important bicyclic system due to their biological activities,[17,18] being a very interesting scaffold in medicinal chemistry, which has been incorporated into many drugs as antitumor[19] and antiviral agents,[20,21] given its ability to mimic the nitrogenous bases of nucleic acids.[17,20] Furthermore, pyrimidodiazepines have shown important activity as Aurora A/B,[22]

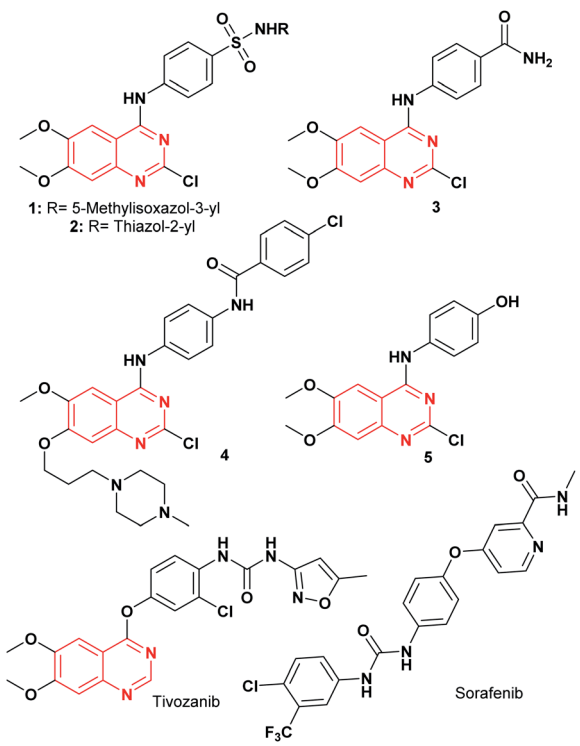

Fig. 2 EGFR and VEGFR-2 tyrosine kinase inhibitors.

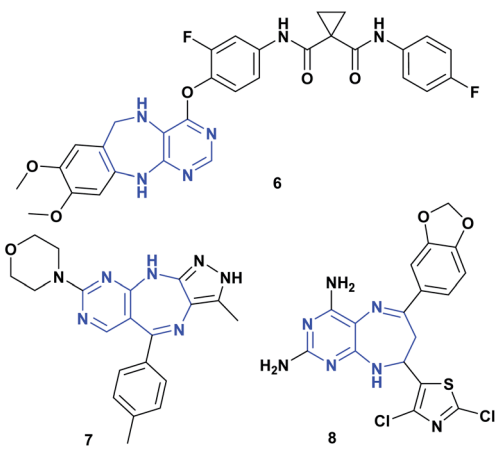

Fig. 3 Pyrimidodiazepines with antitumor activity.

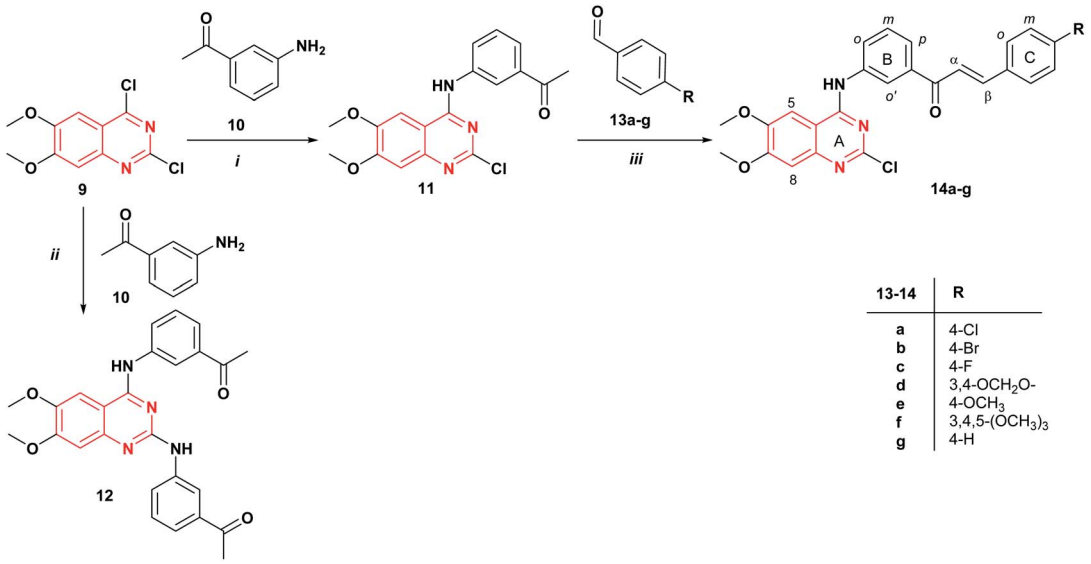

Scheme 1 Synthesis of quinazoline-chalcones **14a–g**. Reagents and conditions: (i) DIPEA, DMF, rt., 24 h; (ii) EtOH, reflux, 4 h; (iii) KOH, MeOH, rt., 24 h.

EGFR,[23] and c-Met kinase[19] inhibitors. Fig. 3 shows some structures of pyrimidodiazepines with significant antitumor activity.[19,22,24]

Based on the general interest of 4-anilinoquinazolines, we designed and synthesized a new series of pyrimidodiazepines containing the 2-chloro-4-anilinoquinazoline fragment, which were obtained by the cyclocondensation reaction between quinazoline-chalcones with tetraaminopyrimidine. Further, those quinazoline-chalcones and pyrimidodiazepines were tested for *in vitro* antitumor activity against a wide panel of tumor cells by the U.S. National Cancer Institute (NCI). DNA binding study was carried out between quinazoline derivatives with calf thymus DNA (ctDNA). Moreover, the binding modes of quinazoline derivatives to DNA, EGFR and VEGFR-2 receptors were examined by molecular docking and molecular dynamics studies.

2. Results and discussion

2.1 Chemistry

The synthetic strategy to prepare the target compounds **14** and **16** is illustrated in Schemes 1 and 2. The 2-chloro-4-anilinoquinazoline **11** was obtained *via* nucleophilic substitution of the more reactive 4-chlorine[12,25] of commercially available 2,4-dichloro-6,7-dimethoxyquinazoline **9** with the 3′-aminoacetophenone **10** at room temperature in THF with the addition of DIPEA to afford the desired product **11** in 40% yield (Scheme 1). Further, when the reaction was carried out using DIPEA in DMF, compound **11** was obtained in 45% yield. The mass spectrum of 2-chloro-4-anilinoquinazoline **11** revealed the isotopic profile for a monochloride molecule at *m*/*z* 357/359 $[M]^+/[M+2]^+$ with a 3 : 1 relative abundance (82/27) for ^{35}Cl and ^{37}Cl isotopes. It should be mentioned that the use of ethanol as a solvent under reflux for 4 h, gives the corresponding 2,4-diaminoquinazoline derivative **12** in 63% yield. Thus, quinazoline-chalcones **14a–g** were synthesized in good yields (51–85%) by Claisen–Schmidt condensation between compound **11** and aromatic aldehydes **13a–g** in presence of KOH in methanol at room temperature for 24 h.

The structural elucidation of quinazoline-chalcones **14a–g** was performed by spectroscopic techniques: Fourier-transform infrared spectroscopy (FT-IR), ^1H NMR, ^{13}C NMR, and mass spectrometry. Compounds **14a–g** showed similar spectroscopic data and therefore, we discuss here the compound **14a** as the representative of this series. In the ^1H NMR spectrum, the signal corresponding to Hα appears as a doublet at 7.78 ppm with coupling constant ^3J = 15.5 Hz, confirming the *E*

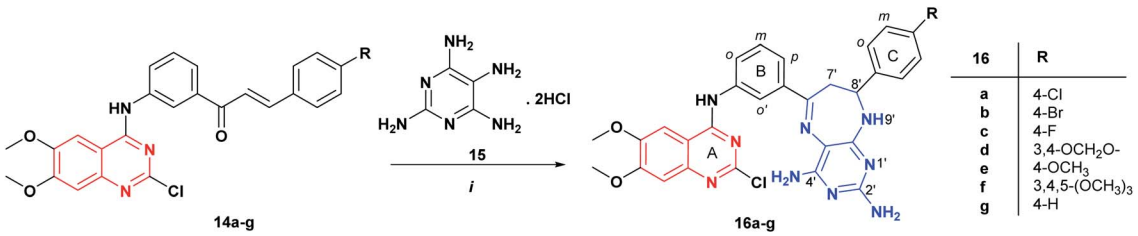

Scheme 2 Synthesis of new pyrimidodiazepines **16a–g** containing the 2-chloro-4-anilinoquinazoline fragment. Reagents and conditions: (i) MeOH, reflux, 10–12 h.

configuration of the C=C bond in the α,β-unsaturated fragment; the signals for Hβ, H-5, H_{Co} and H_{Bp} appear as a multiplet between 8.06–7.84 ppm. At 3.97 and 3.93 ppm, two singlets were assigned to the methoxy groups. The ^{13}C NMR spectrum showed the expected twenty-three signals for the carbon atoms of compound **14a**. The mass spectrum showed the molecular ion peak at *m*/*z* 479/481/483 with a isotopic profile (12/11/1) $[M]^+/[M+2]^+/[M+4]^+$, according to the assigned structure.

The reaction of quinazoline-chalcones **14a–g** with 2,4,5,6-tetraaminopyrimidine dihydrochloride **15** in methanol under reflux leads to the regioselective formation of a new series of pyrimidodiazepine derivatives **16a–g** in good yields (50–58%). In this case, the reaction is highly regioselective, being controlled by nucleophilic addition of the more nucleophilic 5-amino group of the tetraaminopyrimidine **15** to the carbonyl group of the α,β-unsaturated fragment of **14** followed by a Michael type addition to Cβ of **14a–g**, in agreement with the previously reported works on the synthesis of pyrimidodiazepines.[24,26,27] The structural assignment of compounds **16a–g** was performed based on NMR data, and mass spectrometry. In the ^{1}H NMR spectrum of compound **16b**, the signals for H-7 appear as a double doublet and multiplet at 2.83 ppm integrating for one proton ($H_{7a'}$) and between 3.94–3.84 ppm for four protons corresponding to H-7′ ($H_{7b'}$) and the OCH_3 protons, and the signal of H-8′ appears as a triplet at 5.05 ppm with coupling constant $^3J = 5.8$ Hz, which form an AMX spin systems. Two singlets for the amino protons 2′-NH_2 and 4′-NH_2 were observed at 5.75 and 6.27 ppm, respectively. The ^{13}C NMR spectrum showed the expected twenty-seven signals for the carbon atoms of compound **16b**.

2.2 Anticancer activity

Quinazoline derivatives **14a–g** and **16a–g** were submitted to Developmental Therapeutic Program (DTP) of the U.S. National Cancer Institute (NCI). All compounds (**14a–g** and **16a–g**) were selected for anticancer evaluation against 60 cancer cell lines of different panels of human tumor including colon, lung, prostate, ovarian, breast, and renal carcinoma, melanoma, central nervous system tumors, and leukemia. The preliminary *in vitro* anticancer screening was carried out at a single-dose of 10 μM after 48 h of incubation with the tumor cell lines. The results were reported as percentages growth (*G*%) (values between 0 and 100) and lethality (values less than 0) of the treated cells *vs.* control cells by the COMPARE program (see ESI†). Table 1 shows the results of antiproliferative activity expressed in terms of percent growth inhibition (GI% = 100 − *G*%) and lethality.[28] Compounds **14g**, **16a**, and **16c** were found to be highly active because they exhibited significant growth inhibition with the lowest values of mean growth (52.70, 46.58, and 57.99%, respectively) and high percentages growth inhibition (GI%), including lethality values in some cell lines, especially on HCT-

Table 1 Anticancer activity of quinazolines **14a–g** and **16a–g** against NCI 60 human cancer cell lines at one-dose (10 μM)

Compound	NSC Number	Mean growth	Most sensitive cell lines	*G*%/lethality[a]	GI%[b]
14a	822717	64.03	HCT-116 (colon cancer)	**−0.90**	—
			SW-620 (colon cancer)	**−5.87**	—
14b	822718	79.02	RPMI-8226 (leukemia)	**−2.21**	—
14c	822719	57.88	RPMI-8226 (leukemia)	**−18.09**	—
			HCT-116 (colon cancer)	**−41.24**	—
14d	822720	96.91	RPMI-8226 (leukemia)	26.65	**73.35**
14e	822721	85.65	RPMI-8226 (leukemia)	18.57	**81.43**
14f	822722	81.23	RPMI-8226 (leukemia)	13.87	**86.13**
14g	*822723*	***52.70***	*RPMI-8226 (leukemia)*	***−2.13***	—
			HCT-116 (colon cancer)	***−52.14***	—
			HCT-15 (colon cancer)	***−34.08***	—
			SW-620 (colon cancer)	***−11.91***	—
16a	*826382*	***46.58***	*CCFR-CEM (leukemia)*	***−30.26***	—
			HCT-116 (colon cancer)	***−44.82***	—
			U251 (CNS cancer)	***−52.44***	—
			LOX IMVI (melanoma)	***−52.35***	—
			786-0 (renal cancer)	***−52.06***	—
16b	826383	68.59	U251 (CNS cancer)	**−46.46**	—
16c	*826384*	***57.99***	*HCT-116 (colon cancer)*	***−41.74***	—
			U251 (CNS cancer)	***−22.02***	—
			LOX IMVI (melanoma)	***−53.62***	—
			MCF7 (breast cancer)	***−5.06***	—
16d	826385	71.80	U251 (CNS cancer)	8.17	**91.83**
16e	826386	76.27	SR (leukemia)	3.81	**96.19**
16f	826387	93.37	K-562 (leukemia)	55.33	44.67
16g	826388	81.09	K-562 (leukemia)	6.71	**93.29**
			SR (leukemia)	**−1.18**	—

[a] *G*%, growth percentages (values between 0 and 100); lethality, values less than 0. [b] GI, growth inhibition percentages (GI% = 100 − *G*%). Bold values correspond to GI > 50 (active compound against that cell line). The most active compounds are highlighted in italic.

Table 2 Anticancer activity of compounds **14g**, **16a** and **16c** at five-dose expressed in GI_{50}, TGI and LC_{50} (μM)[a]

	Compounds									Doxorubicin NSC 123127[b]		
	14g			**16a**			**16c**					
Panel cell line	GI_{50}	TGI	LC_{50}	GI_{50}	TGI	LC_{50}	GI_{50}	TGI	LC_{50}	GI_{50}	TGI	LC_{50}
Leukemia												
CCRF-CEM	2.45	>100	>100	1.59	**5.30**	>100	1.05	**4.14**	>100	0.081	10.0	100
HL-60(TB)	3.61	>100	>100	1.79	4.18	**9.77**	1.95	4.09	**8.60**	0.120	2.57	89.1
K-562	1.74	>100	>100	1.91	**4.16**	**9.08**	1.96	**4.69**	>100	0.194	12.0	100
MOLT-4	2.77	>100	>100	1.75	5.10	>100	1.77	5.45	>100	0.031	1.00	100
RPMI-8226	0.622	3.48	>100	1.97	4.84	>100	1.77	4.42	>100	0.076	1.28	100
SR	1.70	—	>100	1.91	5.33	>100	1.96	4.80	>100	0.028	1.34	100
Non-small cell lung cancer												
A549/ATCC	15.00	>100	>100	3.14	16.10	>100	2.64	7.82	>100	0.061	0.28	100
EKVX	11.40	>100	>100	2.44	9.17	>100	1.50	**3.99**	>100	0.416	5.49	47.8
HOP-62	3.71	31.7	>100	5.24	32.50	>100	1.68	3.69	—	0.067	1.99	67.6
HOP-92	2.09	8.51	>100	1.68	3.82	—	1.50	3.72	—	0.100	1.99	42.6
NCI-H226	5.81	>100	>100	14.90	50.1	>100	3.22	16.60	>100	0.050	0.25	6.45
NCI-H23	6.62	>100	>100	2.69	8.40	>100	2.00	4.73	>100	0.151	0.91	13.1
NCI-H322M	20.40	>100	>100	2.93	9.91	>100	2.14	5.57	**34.8**	0.537	5.01	67.6
NCI-H460	4.20	>100	>100	2.01	3.87	—	1.91	3.82	**7.64**	0.017	1.28	51.2
NCI-H522	3.09	52.6	>100	—	—	—	—	—	—	0.028	0.16	2.81
Colon cancer												
COLO 205	11.40	>100	>100	1.80	3.81	—	1.77	3.51	6.94	0.181	0.95	4.36
HCC-2998	2.54	5.56	>100	1.89	3.63	—	1.92	3.48	**6.32**	0.257	2.23	21.8
HCT-116	1.62	**5.16**	>100	1.71	**3.25**	—	1.76	**3.34**	**6.33**	0.079	8.12	54.9
HCT-15	**2.88**	>100	>100	**2.07**	**4.80**	>100	**1.96**	**4.27**	**9.27**	6.45	100	100
HT29	4.39	>100	>100	2.05	4.53	>100	2.05	4.38	**9.34**	0.123	0.95	67.6
KM12	2.45	>100	>100	1.94	**3.88**	—	1.88	**3.61**	**6.94**	0.263	14.7	93.3
SW-620	2.79	>100	>100	1.85	**3.79**	**7.78**	1.76	**3.60**	**7.39**	0.091	11.7	58.8
CNS cancer												
SF-268	4.99	81.40	>100	1.85	4.05	—	1.68	3.68	**8.07**	0.104	1.41	30.1
SF-295	3.08	19.60	>100	1.89	3.78	—	1.82	3.50	**6.72**	0.102	1.25	69.1
SF-539	3.82	19.20	>100	1.75	3.13	5.71	1.53	2.93	**5.60**	0.114	1.51	26.9
SNB-19	2.89	10.10	>100	1.99	4.22	—	1.94	4.22	—	0.042	2.63	50.1
SNB-75	2.06	8.61	>100	2.39	14.30	63.90	1.13	2.42	5.19	0.067	0.33	3.31
U251	3.11	14.50	>100	1.99	4.20	—	2.12	4.35	—	0.038	2.23	30.9
Melanoma												
LOX IMVI	1.54	3.63	>100	1.87	3.79	—	1.78	3.51	**6.93**	0.066	2.45	50.1
M14	5.01	>100	>100	1.87	4.04	—	1.86	3.70	7.36	0.123	0.41	3.98
MDA-MB-435	3.40	28.90	>100	1.64	3.07	5.77	1.66	3.11	5.84	0.177	0.93	4.07
SK-MEL-2	4.42	57.70	>100	1.95	4.21	—	1.65	3.68	—	0.251	1.44	9.54
SK-MEL-28	5.03	>100	>100	1.66	3.10	5.78	1.62	3.04	5.69	0.169	0.39	1.07
SK-MEL-5	5.17	>100	>100	1.68	3.08	5.62	1.65	3.02	**5.51**	0.208	0.70	15.8
UACC-257	9.75	>100	>100	2.43	6.22	>100	1.96	3.94	7.94	0.077	0.21	0.48
UACC-62	2.55	10.10	>100	1.71	3.32	—	1.76	3.31	**6.23**	0.141	0.47	8.12
Ovarian cancer												
IGROV1	4.45	42.90	>100	2.90	**10.90**	>100	1.78	**4.16**	—	0.169	12.8	100
OVCAR-3	3.75	31.30	>100	2.04	**4.20**	**8.63**	1.85	**3.55**	**6.79**	0.389	10.0	85.1
OVCAR-4	5.50	33.30	>100	2.00	**4.81**	**19.30**	1.63	**3.38**	**7.03**	0.371	7.41	74.1
OVCAR-5	8.79	>100	>100	2.12	5.25	**22.40**	1.79	**3.55**	**7.04**	0.416	4.67	100
OVCAR-8	4.99	>100	>100	2.35	5.99	>100	2.30	—	>100	0.100	1.99	43.6
NCI/ADR-RES	7.26	>100	>100	4.16	92.00	>100	6.07	>100	>100	7.24	72.4	100
SK-OV-3	7.96	51.70	>100	21.80	48.00	>100	25.70	59.20	>100	0.223	13.1	100
Renal cancer												
786-0	3.05	15.00	>100	1.70	**3.18**	—	1.56	**2.99**	**5.71**	0.125	5.62	51.2
A498	6.23	44.3	>100	10.50	26.90	69.20	1.01	2.47	6.00	0.100	0.38	1.90
ACHN	3.51	>100	>100	2.15	**4.87**	**15.20**	1.74	**3.22**	**5.97**	0.075	13.8	100

Table 2 (*Contd.*)

	Compounds											
	14g			**16a**			**16c**			Doxorubicin NSC 123127[b]		
Panel cell line	GI_{50}	TGI	LC_{50}	GI_{50}	TGI	LC_{50}	GI_{50}	TGI	LC_{50}	GI_{50}	TGI	LC_{50}
CAKI-1	4.17	**35.40**	>100	1.99	**4.49**	**11.50**	1.61	**3.27**	**6.64**	0.954	56.2	100
RXF 393	2.02	5.46	>100	1.61	3.14	—	1.38	2.85	—	0.097	0.53	4.67
SN12C	3.98	41.10	>100	2.68	8.10	81.40	1.72	**3.48**	**7.05**	0.072	5.01	72.4
TK-10	4.19	20.00	>100	2.62	6.87	>100	1.95	3.86	**7.63**	0.186	2.39	87.0
UO-31	17.8	>100	>100	2.48	8.89	76.40	1.55	3.54	**8.07**	0.489	2.63	26.3
Prostate cancer												
PC-3	3.86	27.80	>100	3.97	37.90	>100	2.17	6.68	>100	0.323	5.88	87.0
DU-145	23.80	>100	>100	2.07	**8.84**	**17.60**	1.77	**3.44**	**6.67**	0.107	17.7	100
Breast cancer												
MCF7	1.81	>100	>100	1.80	**4.11**	—	1.73	**3.92**	—	0.027	10.7	51.2
MDA-MB-231/ATCC	9.14	85.40	>100	1.63	**3.29**	**6.64**	1.49	**3.03**	**6.14**	0.512	4.16	34.6
HS 578T	3.71	41.10	>100	1.88	**4.28**	—	1.98	**4.53**	>100	0.331	4.67	85.1
BT-549	2.36	7.83	53.6	7.93	38.00	>100	2.29	4.36	**8.33**	0.234	2.18	21.3
T-47D	9.17	>100	>100	2.02	4.61	>100	1.93	4.64	>100	0.058	0.77	85.1
MDA-MB-468	3.39	>100	>100	1.73	3.49	7.05	1.79	3.39	6.42	0.055	0.31	2.51
MEAN	4.07	4.27	100	2.34	6.17	39.8	1.91	4.36	15.5	0.141	2.34	28.8

[a] GI_{50}, the molar concentration of compound required to inhibit 50% of the growth of the cancer cell line (relative to untreated cells); TGI, the molar concentration leading to total growth inhibition; and LC_{50}, the molar concentration required to kill 50% of cancer cells. [b] The values of activity against human cancer cell lines displayed by adriamycin/doxorubicin (NSC 123127). Please visit: https://dtp.cancer.gov/dtpstandard/cancerscreeningdata/index.jsp. Bold values are the highest values of GI_{50}, TGI and LC_{50} in comparison to the standard anticancer agent adriamycin/doxorubicin.

116 (colon cancer), U251 (CNS cancer) and LOX IMVI (melanoma), respectively. Compound **14g** showed strong growth inhibition in the three colon cancer cell lines HCT-116, HCT-15 and W-620 with 52.14, 34.08 and 11.91% lethality. Whereas **16a** exhibited high inhibitory effects on the cancer cell lines HCT-116 (colon cancer), U251 (CNS cancer), LOX IMVI (melanoma) and 786-0 (renal cancer) with 44.82, 52.44, 52.35 and 52.06% lethality, respectively. Compound **16c** showed a significant antiproliferative effect on HCT-116 (colon cancer), U251 (CNS cancer), LOX IMVI (melanoma) and MCF7 (breast cancer). On the other hand, the introduction of methylenedioxy (**14d**, **16d**) and methoxy (**14e**, **14f**, **16e**, **16f**) groups on the aryl ring (C, Schemes1 and 2) was unfavorable (high mean growth values), resulting in a reduced antiproliferative activity.

Subsequently, compounds **14g**, **16a**, and **16c** were selected for advanced five-dose testing against the above 60 cancer cell lines using a series of five 10-fold dilutions (100.0, 10.0, 1.0, 0.1, 0.01 μM).[29,30] The results were expressed for each cell line in three dose–response parameters, GI_{50} (molar concentration of compound required to inhibit 50% of the growth of the cancer cell line), TGI (molar concentration leading to total growth inhibition), and LC_{50} (molar concentration required to kill 50% of cancer cells).[31]

As illustrated in Table 2, the quinazoline-chalcone **14g** displayed high antiproliferative activity on K-562 (leukemia), RPMI-8226 (leukemia), HCT-116 (colon cancer), LOX IMVI (melanoma) and MCF7 (breast cancer) cancer cell lines with GI_{50} values between 0.622–1.81 μM. It exhibited strong growth inhibitory activity against the K-562 leukemia cell line with GI_{50} of 0.622 μM. Compound **16a** exhibited potent anticancer activity against the cell lines HL-60(TB) (leukemia), K-562 (leukemia), HCT-116 (colon cancer), HCT-15 (colon cancer), SW-620 (colon cancer), SF-539 (CNS cancer), SK-MEL-5 (melanoma), OVCAR-3 (ovarian cancer), OVCAR-4 (ovarian cancer), ACHN (renal cancer), CAKI-1 (renal cancer), DU-145 (prostate cancer), MCF7 (breast cancer), MDA-MB-231/ATCC (breast cancer) and MDA-MB-468 (breast cancer), showing for those cell lines better cytostatic (TGI) and/or cytotoxic activity (LC_{50}) than adriamycin/doxorubicin (**NSC 123127**), NCI standard drug. Moreover, compound **16c** exhibited the highest cytostatic activity against SNB-75 (CNS cancer) and 786-0 (renal cancer) cells line with TGI value of 2.42 and 2.99 μM. It totally inhibited the growth of thirty-six (36) cell lines at 2.42–3.99 μM. As a reference, the growth inhibition percentages of compound **16c** against the 60 cancer cell lines at five different concentrations were recorded in dose–responses curves (Fig. 4).

Among those molecules, compound **16c** also displayed 10.0-fold higher cytotoxic activity against ten cell lines in comparison to the standard anticancer agent adriamycin/doxorubicin (**NSC 123127**) for HL-60(TB) (leukemia), HCT-15 (colon cancer), OVCAR-3 (ovarian cancer), OVCAR-4 (ovarian cancer), OVCAR-5 (ovarian cancer), ACHN (renal cancer), CAKI-1 (renal cancer), SN12C (renal cancer), TK-10 (renal cancer) and DU-145 (prostate cancer) cell lines with LC_{50} values ranging from 5.97 to 9.27 μM. Given their antitumor activities, compounds **14g**, **16a** and **16c**

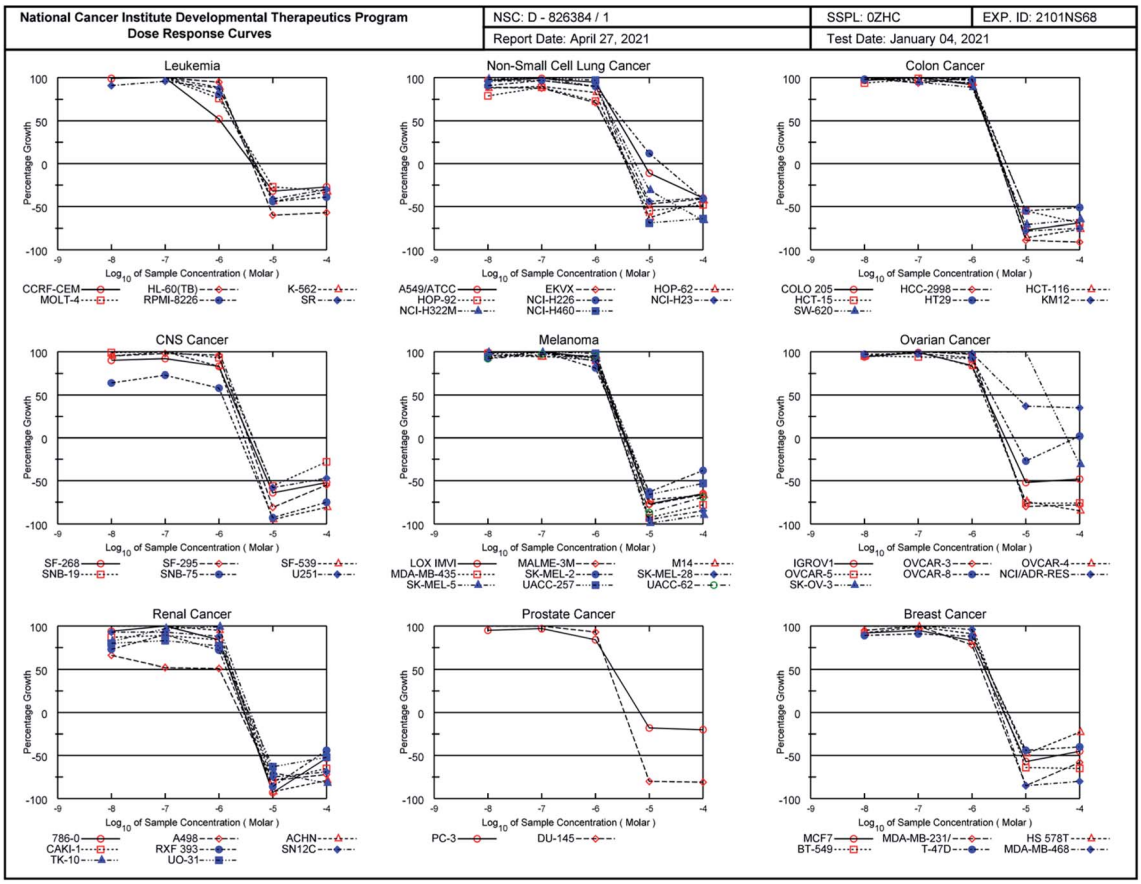

Fig. 4 Anticancer activity of compound **16c** against 60 cancer cell lines of different panels of human cell lines. The horizontal lines at zero (0) show the concentration that leads to total growth inhibition.

were further tested for hemolytic activity against human red blood cells (huRBC). None of the active compounds induced disruption of human red blood cells (0.0–0.6%), indicating that they may be not related with cell membrane damage.

2.3 COMPARE analysis

The NCI COMPARE algorithm (https://dtp.cancer.gov/databases_tools/compare.htm) indicates a correlation between compounds with known biological targets, which have been used extensively to predict and identify the mechanisms of action of synthetic and natural products.[32–34] Therefore, the *in vitro* antitumor screening of compounds **14g**, **16a** and **16c** were analyzed using COMPARE algorithm against the NCI *standard drugs* database at the GI_{50} and LC_{50} levels. The algorithm ranks the results of the tested compound in order of the similarity of responses against 60 human tumor cell lines,[31] expressed quantitatively as Pearson correlation coefficient (PCC) as shown in Table 3. Compounds **14g**, **16a**, and **16c** showed low Pearson correlation coefficients (PCC) did not allow to distinguish their antiproliferative mechanism (end point – GI_{50}). However, compound **16c** showed the highest correlation at the LC_{50} level with the DNA alkylating agent CCNU (lomustine) (**NSC 79037**)

Table 3 COMPARE results list for compounds **14g**, **16a** and **16c**

Compound	End point	PCC[a]	Target	NSC number	Target/mechanism of action
14g	GI_{50}	0.58	L-Cysteine analogue	303861	L-Glutamine antagonist inhibited purine nucleotide biosynthesis[35]
16a	GI_{50}	0.58	*S*-Trityl-L-cysteine	83265	Inhibitor of the Human Kinesin Eg5 (ref. 36)
16c	GI_{50}	0.61	Didemnin B	325319	Didemnin B inhibits protein synthesis and **DNA** synthesis[37]
	LC_{50}	0.75	CCNU (lomustine)	79037	**DNA**/**RNA** alkylating agent[38]

[a] PCC: Pearson correlation coefficient (PCC $\geq$ 0.60 was considered significant).

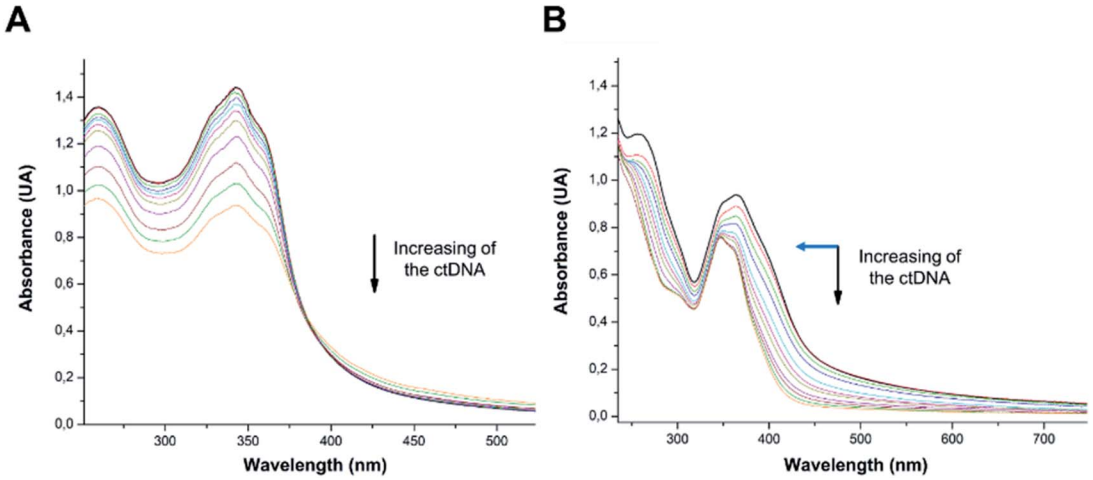

Fig. 5 (A) UV-vis absorption spectra of quinazoline-chalcone **14g** and (B) pyrimidodiazepine **16c** alone (black line) after the addition of amounts of calf thymus DNA (ctDNA) from 9.6 to 96.0 μM (orange line) at 25 °C. The arrow shows the absorbance change by the addition of ctDNA.

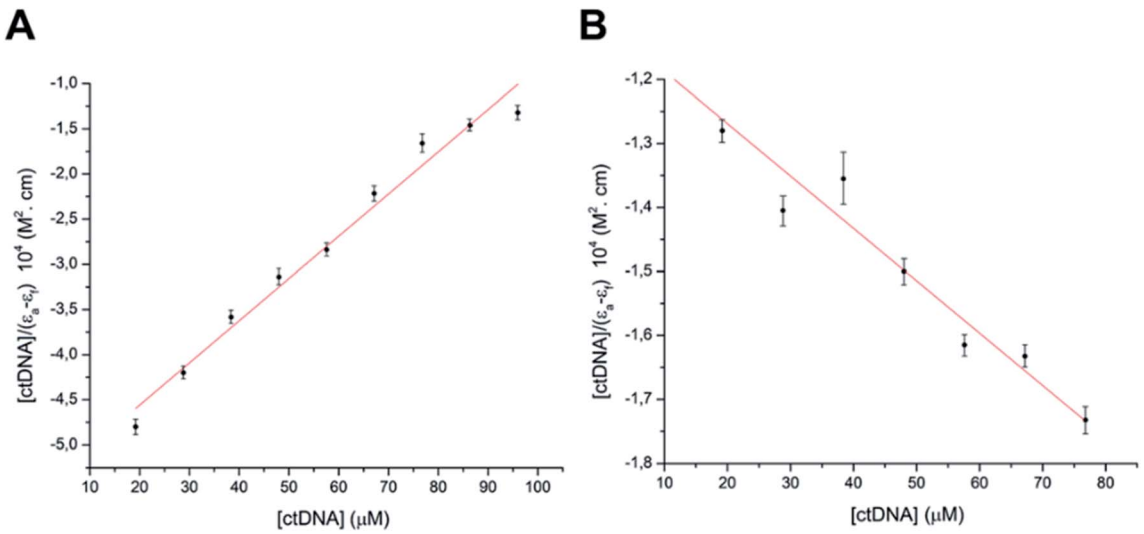

Fig. 6 Binding saturation plots according to Wolfe–Shimmer equation. (A) ctDNA–**14g** and (B) ctDNA–**16c**.

(PCC = 0.75), suggesting that compound **16c** possesses a similar cytotoxicity mechanism of action through DNA binding.

2.4 DNA binding study

According to COMPARE analysis, compound **16c** owes its anticancer activity through DNA binding, being DNA an important target of anticancer agents. Therefore, the study of the union between the quinazolines (**14g** and **16c**) and calf thymus DNA (ctDNA) was carried out by UV spectroscopy to assess the possible interaction between those compounds with nucleic acids. Quinazolines **14g** and **16c** showed alterations on their electronic UV spectra during the titration of a fixed amount of ctDNA. Fig. 5A shows a clear hypochromic effect of up to 35% on the electronic UV spectrum of **14g** after the addition of ctDNA, without showing a significant change in the maximum absorption wavelengths. Besides, an isosbestic point was found at 385 nm, indicating the presence of two species in the solution,[39,40] the free compound **14g** and the **14g**–ctDNA complex. The hypochromic effect indicates that this molecule may interact with the DNA strands by intercalation since the molecular structure of **14g** has a planar conjugated system,

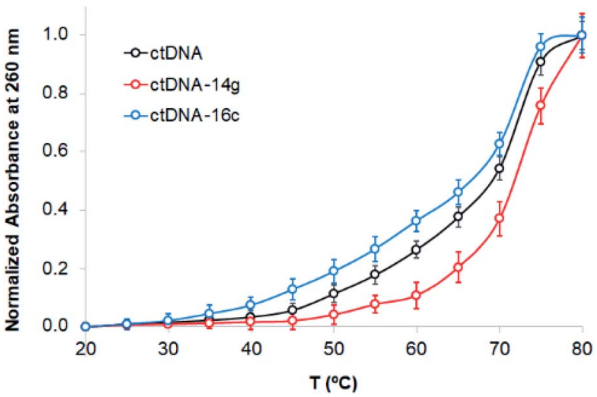

Fig. 7 Melting curves of ctDNA (80 μM) in the absence and presence of the compounds **14g** and **16c** (80 μM).

which facilitates interaction with the double-stranded ctDNA.[41] As shown in Fig. 5B, compound **16c** also shows a hypochromic effect after titration with ctDNA, being up to 19% for the highest concentration of ctDNA evaluated due to the binding mode between the compound **16c** and the nitrogenous bases of DNA through π–π stacking interaction.[41] A clear blue shift in the peak position can be observed in Fig. 5, and this hypsochromism indicates the destabilization of the π interactions involving the nitrogenous bases due to the entry of one-half of the planar molecule, whose second zone has a non-planar steric conformation.[42]

According to UV-vis absorption spectra, the binding constant (K_b) were calculated from Wolfe–Shimmer eqn (1) as 9.3×10^3 and 7.1×10^3 M^{-1} for the compounds **14g** and **16c** with DNA, respectively (Fig. 6), where ε_a, ε_f, and ε_b are apparent molar absorption coefficients of the compound with DNA, without DNA, and binding DNA, respectively.[43,44] The binding constant (K_b) values were higher than those found for the DNA target drugs methyl-CCNU (semustine) and CCNU (lomustine) with K_b of 1.53×10^3 and 8.12×10^3 M^{-1} to calf thymus DNA, respectively.[45] The interactions between small molecules and nucleic acids can generally be classified into two types: intercalation and groove binding; however, some molecules possess structural properties that favor interactions using both mechanisms, such as planarity, high π conjugation, and additional charges or zones that are deficient in high electron density.[14] These results indicated that compounds **14g** and **16c** could bind to the groove of DNA or weak intercalation, where compound **14g** has a higher affinity than **16c** to DNA, according to the hypochromic effect and binding constant (K_b). These findings may contribute to a greater understanding of the mechanism of action of those quinazoline derivatives.

$$\frac{[DNA]}{\varepsilon_a - \varepsilon_f} = \frac{[DNA]}{\varepsilon_b - \varepsilon_f} + \frac{1}{K_b(\varepsilon_b - \varepsilon_f)} \quad (1)$$

The binding of compounds to DNA can alter the denaturation temperature (T_m) of DNA, depending on intercalation forces. Absorbance changes at 260 nm were observed when the absorbance of ctDNA was measured in the absence and presence of the compounds **14g** and **16c**. Fig. 7 presents the melting curves of free ctDNA and its systems, showing that the T_m value

Table 4 Binding energy and type of interactions between ligands and controls with EGFR, VEGFR-2 and DNA[a]

Ligands	Receptor	Binding energy (kcal mol^{-1})	HB	EI	HI	Halogen
Mitoxantrone	DNA	−6.40	3	2	0	0
14g	DNA	−8.30	5	2	0	0
16c	DNA	−8.20	9	2	0	0
Gefitinib	EGFR	−5.40	0	1	5	0
Lapatinib	EGFR	−8.30	3	1	6	1
14g	EGFR	−6.30	8	0	5	0
16a	EGFR	−7.80	3	2	11	0
16c	EGFR	−9.90	5	0	18	1
Sorafenib	VEGFR-2	−9.10	7	0	5	2
Tivozanib	VEGFR-2	−7.70	4	1	6	0
14g	VEGFR-2	−7.90	2	3	6	0
16a	VEGFR-2	−9.20	6	3	2	0
16c	VEGFR-2	−9.00	10	2	5	1

[a] HI: hydrophobic interactions; HB: hydrogen bonds; EI: electrostatic interactions.

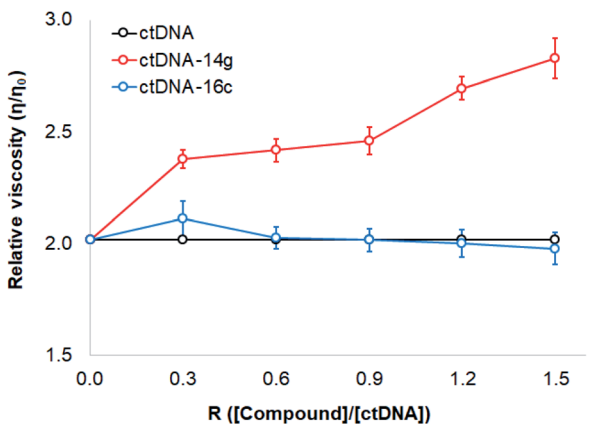

Fig. 8 Effect of increasing amounts of **14g** and **16c** on the relative viscosity of ctDNA.

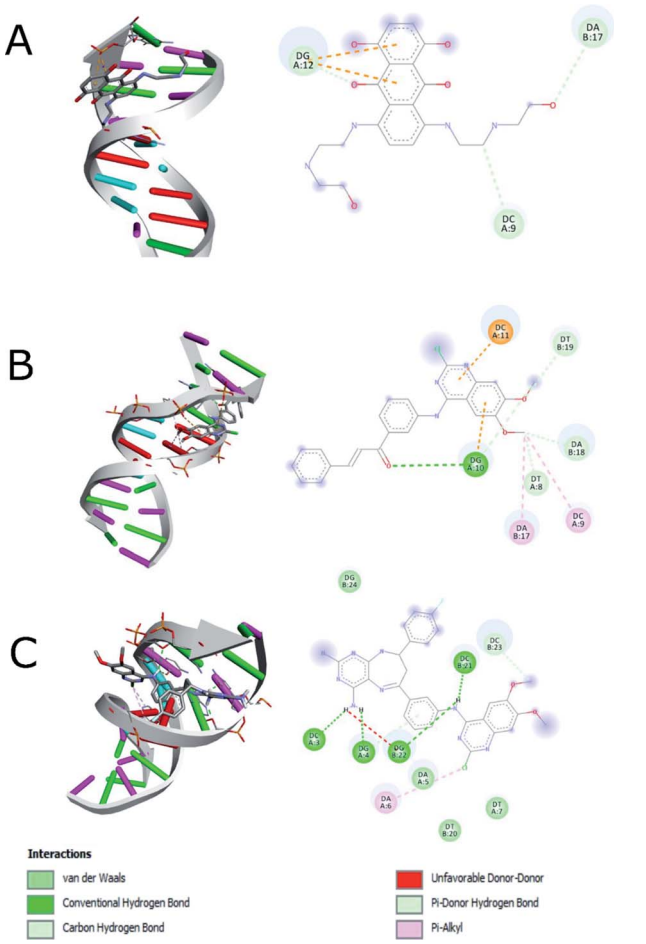

Fig. 9 Interaction between (A) hydrophobic interaction mitoxantrone and DNA, (B) **14g** with DNA and (C) **16c** with DNA.

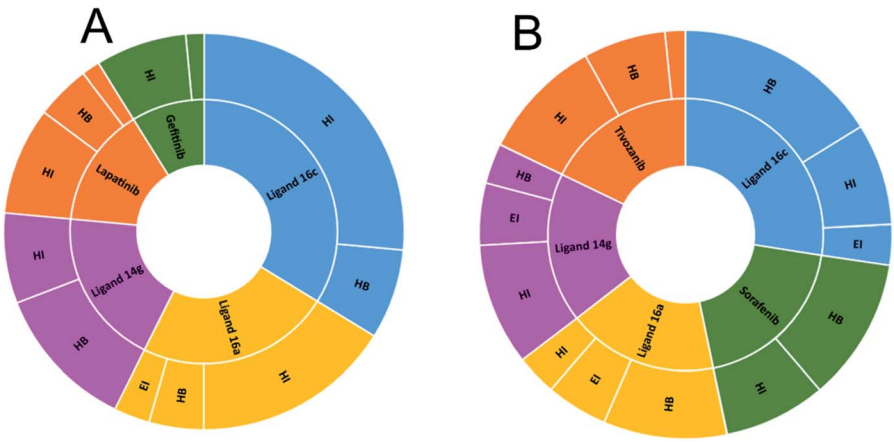

Fig. 10 Number of interactions between ligands and controls with (A) EGFR and (B) VEGFR-2. HI: hydrophobic interactions; HB: hydrogen bonds; EI: electrostatic interactions.

changed from 69 °C for native ctDNA to approximately 72 and 67 °C for ctDNA–**14g** and ctDNA–**16c**, respectively, which suggests that the binding mode involves the destabilization of π interactions, weak intercalation, or unfavorable groove binding.[46] In general, the union between small molecules and DNA that occurs through strong intercalation forces causes T_m values to increase from 5–8 °C;[46,47] therefore, this mode of binding could be excluded.

To study changes in the hydrodynamics of an aqueous DNA solution caused by phenomena related to changes in the DNA length and tertiary structures, viscosity studies were carried out for ctDNA alone and combined with compounds **14g** and **16c** at various concentrations. Fig. 8 displays a graph of the relative viscosity *versus* the [compound]/[ctDNA] ratio. These results indicated that no significant changes occurred in the ctDNA–**16c** system, further supporting that the interaction occurs through groove binding because DNA length remains intact and viscosity is almost unaffected when a molecule binds to the groove of a double-helix DNA molecule.[40] When the ctDNA–**14g** system was examined, an increase in the ctDNA viscosity was observed, which suggested that the **14g** molecules are accommodated in the space of adjacent base pairs, as occurs during classical intercalation binding.[46]

Based on these results, compound **16c** most likely binds ctDNA through a groove interaction, whereas compound **14g** appears to favor weak intercalations at 25 ± 5 °C. To establish the possible interactions of those quinazoline derivatives, molecular docking was performed with DNA, EGFR, and VEGFR-2 receptors.

2.5 Molecular docking

The docking study was performed on DNA to predict the binding affinity and the interactions of compounds **14g** and **16c** using mitoxantrone[48,49] for interaction with DNA (1BNA). Based on the fact that 2-chloro-4-anilinoquinazoline derivatives have been reported as anticancer agents to target the EGFR and VEGFR-2 receptors,[9,12,13] we also performed the studies of docking of compounds **14g**, **16a** and **16c** into the active site of the EGFR (PDB: 1XKK) and VEGFR-2 (PDB: 4ASE). Two controls were taken for both EGFR (gefitinib and lapatinib) and VEGFR-2 (sorafenib and tivozanib) receptors. The structures of the compounds **14g**, **16a** and **16c** (ligands) and controls were prepared with Autodock software[50] using Gasteiger charges.[51]

As shown in Table 4, a comparison of the interactions with DNA between mitoxantrone (DNA intercalating agent) and

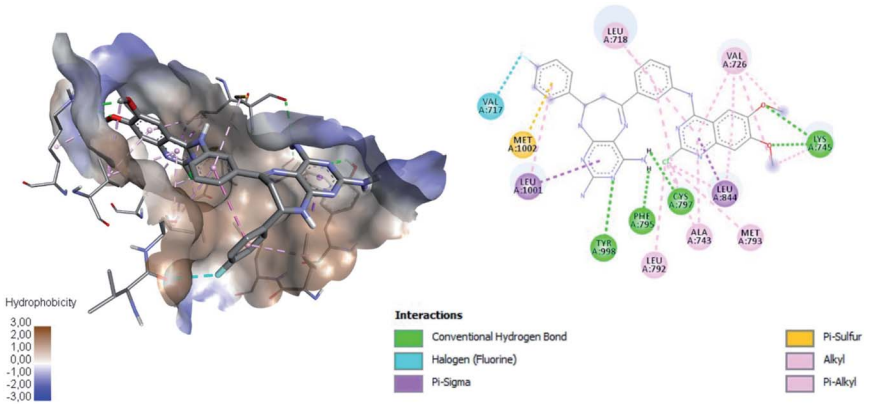

Fig. 11 Interaction between **16c** and EGFR using the hydrophobicity scale and 2D plot.

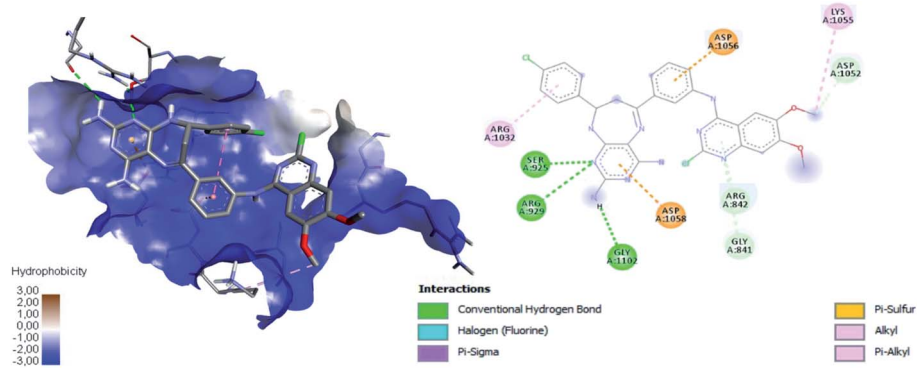

Fig. 12 Interaction between **16a** and VEGFR-2 using the hydrophobicity scale and 2D plot.

compound **16c**, shows that **16c** exhibits an enhanced interaction with a binding energy of −8.20 kcal mol^{-1} mainly hydrogen bonding type interaction with the 4-amino group of pyrimidodiazepine **16c** (dashed lines in Fig. 9). In contrast, the quinazoline-chalcone **14g** was the structure that interacts most strongly with DNA, forming both hydrogen bonds and hydrophobic interactions, generating a slightly better binding energy of −8.30 kcal mol^{-1} with respect to ligand **16c** (−8.20 kcal mol^{-1}), which agrees quite well with the results obtained for compound **14g** with calf thymus DNA by UV spectroscopy.

Fig. 9 shows the enhanced interaction of the compound **16c** with DNA by forming mainly hydrogen bonds from the amino groups of pyrimidodiazepine and anilino moieties with both cytosine (Dc3, Dc21) and guanine (Dg4, Dg22). Further, the 2-chlorine atom of quinazoline of **16c** allows it to form hydrophobic interactions with adenine (Da6) to a lesser degree. In contrast, the quinazoline moiety of ligand **14g** interacts with hydrogen bond, electrostatic and hydrophobic interactions with all nitrogenous bases bind to the minor groove of DNA as revealed from the most favorable conformation of the docking study (Fig. 9B). The hydrogen bond was formed between the carbonyl group of the α,β-unsaturated fragment with guanine (Dg10). Mitoxantrone exhibits only two hydrophobic interactions with guanine (Dg12).

Table 4 shows how ligand **16c** has higher binding energy with the EGFR receptor, even better than the controls lapatinib and gefitinib. The type of interactions that ligand **16c** presented were mainly 18 hydrophobic interactions, five hydrogen bridges, and one halogenated. Hydrophobic interactions are formed with quinazoline moiety of **16c** where 2-chlorine atom increases this type of interaction forming up to five hydrophobic interactions mainly with Ala743, Leu792, and Met793. Regarding the affinity between ligand and VEGFR-2 the best result was found for compound **16a** (−9.20 kcal mol^{-1}), followed closely by **16c** (−9.00 kcal mol^{-1}) having similar values to the control sorafenib. The major type of interactions that both ligands **16a** and **16c** displayed with VEGFR-2 were hydrogen bonds.

Fig. 10A shows the interactions between the ligands with the EGFR receptor, where ligands display in common both hydrogen bonding and hydrophobic interactions. Compound **16c** presents a higher number of hydrophobic interactions than the rest of the molecules, followed by ligand **16a** with the same behavior. In Fig. 10B, more hydrogen bridge interactions with the VEGFR-2 receptor are observed among all the ligands except for tivozanib and **14g**, which obtained the lowest affinity energy.

Fig. 11 shows ligand **16c** interacting with EGFR revealing a cavity formed by hydrophobic amino acids such as Val726, Leu792, Leu718, Ala743, Met793, Leu844, and Leu1001 that form hydrophobic interactions with this ligand. Other types of molecular interactions formed are hydrogen bonds with residues such as Lys745, Phe795, Cys797, and Tyr998; besides a halogenated interaction between the 2-chlorine atom of quinazoline **16c** with residue Val717 is formed (Fig. 11).

Fig. 12 shows the interaction between compound **16a** and VEGFR-2, which was the molecule with the best binding energy to the VEGFR-2 receptor, showing a hydrophilic environment compared to the hydrophobic environment of the previous interaction between **16c** and EGFR. The residues that interact

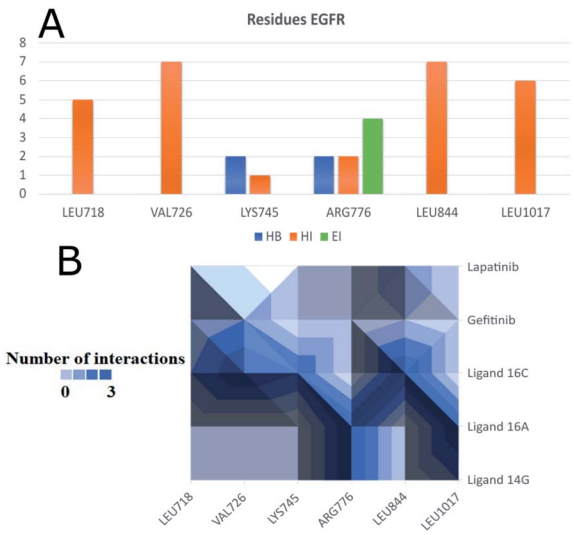

Fig. 13 Most frequent residues in interactions with the EGFR receptor. (A) Most frequent residues in interacting with EGFR and the type of interaction. (B) Heatmap of most frequent residues interacting with ligands and controls. HI: hydrophobic interactions; HB: hydrogen bonds; EI: electrostatic interactions.

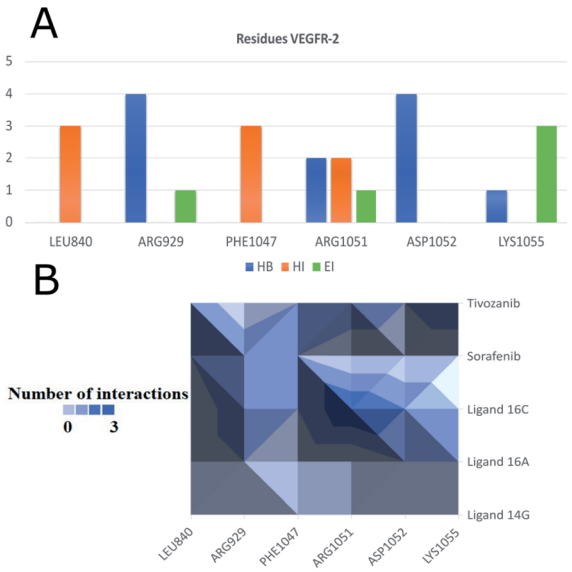

Fig. 14 Most frequent residues in interactions with the VEGFR-2 receptor. (A) Most frequent residues in interacting with VEGFR-2 and the type of interaction. (B) Heatmap of most frequent residues interacting with ligands and controls. HI: hydrophobic interactions; HB: hydrogen bonds; EI: electrostatic interactions.

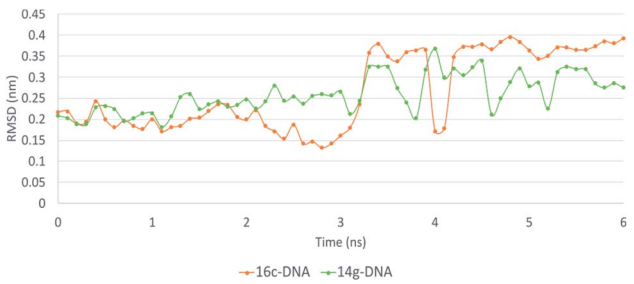

Fig. 15 RMSD of ligand interactions **14g**-DNA and **16c**-DNA.

forming mainly hydrogen bonds with this compound **16a** are Ser925, Arg929, Gly1102, Gly841, Asp1052, and Arg842 (Fig. 12). A few hydrophobic interactions are formed with Arg1032 and Lys1055.

To observe if there are residues in common between the interactions of the ligands with EGFR and VEGFR-2 receptors, Fig. 13 and 14 were made with compounds **14g**, **16a** and **16c**. Fig. 13A shows that Arg776 from the EGFR receptor has the most varied interactions because it presents hydrogen bridges, electrostatic and hydrophobic interactions mainly with ligands **14g** and **16a**. Leu1017 is interacting with ligands **14g** and **16a** through hydrophobic interactions. Compounds **16a** and **16c** share hydrophobic interaction with residue Leu844. Fig. 13B shows that **16a** shares residues in common with **14g** such as Arg776 and Leu1017.

Fig. 14 shows the residues that have the most interactions with VEGFR-2 and ligands including the controls sorafenib and tivozanib. Arg1051 comes to form three different interactions, hydrogen bridges, electrostatic and hydrophobic interactions, mainly with ligand **16c** and tivozanib. The highest number of interactions (4) of the Arg929 ligand has been with ligands **16a**, **16c** and sorafenib. Similarly, residue Asp1052 forms a total of four interactions with ligands **16a**, **16c** and tivozanib.

2.6 Molecular dynamics studies

The MD simulation of ligands **14g** and **16c** with DNA was performed to investigate the DNA-ligand interactions. Fig. 15 shows the RMSD of both molecules, being stable during the first 2 ns. Ligand **14g** from 3 ns onwards starts to vary the stability of its structure by 0.10 nm approximately until 6 ns, this could be due to the intermittent interaction with DNA and surrounding water molecules. Fig. 16 shows the interactions of ligand **14g** with DNA for 6 ns. Up to 4 ns, there is an interaction between the compound **14g** and the nitrogenous bases adenine, cytosine, and guanine through hydrogen bonds is observed.

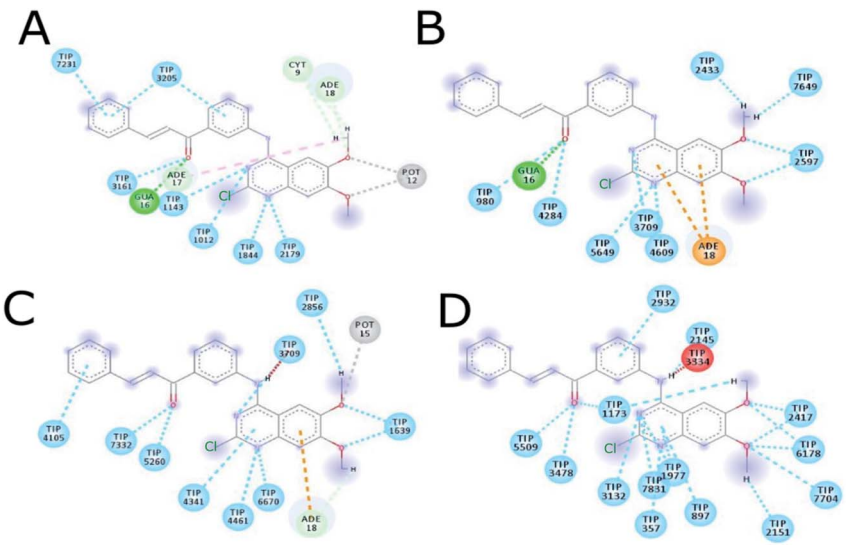

Fig. 16 Intermolecular interactions between **14g** and DNA. (A) 1 ns, (B) 2 ns, (C) 4 ns, (D) 6 ns. CYT: cytosine, GUA: guanine, TIP: water molecule, POT: potassium ion.

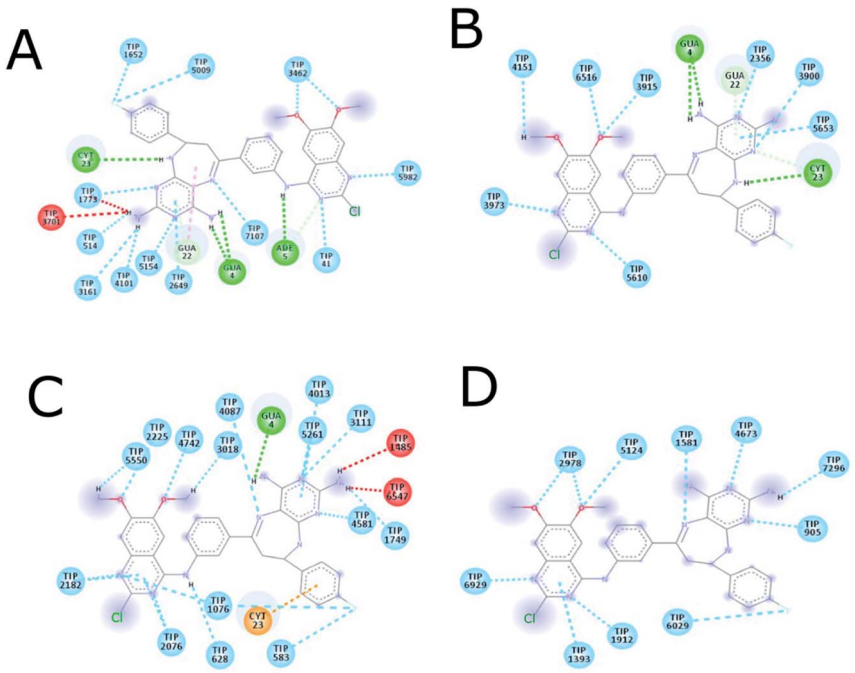

Fig. 17 Intermolecular interactions between **16c** and DNA. (A) 1 ns, (B) 2 ns, (C) 4 ns, (D) 6 ns. ADE: adenine; CYT: cytosine; GUA: guanine; TIP: water molecule.

However, at 6 ns the interaction with DNA stopped and the ligand **14g** only form hydrogen bonds with water. Ligand **16c** presents two peaks at 3 and 4 ns going from 0.14 to 0.35 nm due to high interaction with water molecules as shown in Fig. 15, also there are interactions between the pyrimidodiazepine moiety of ligand **16c** with cytosine and guanine up to 6 ns, then it interacts mainly with water molecules. A transient interaction with DNA is observed (Fig. 17).

Fig. 18 shows the frequency of the type of interaction between **14g** and **16c** with DNA. Hydrogen bonds are the most frequent in the interactions of ligands **14g** and **16c** with DNA, followed by a higher frequency of the interaction with water molecules. Halogenated bond formation is also observed by the 2-chlorine atom of quinazoline present in the **16c** for the interaction with DNA. If we compare to which type of nitrogenous bases ligands **14g** and **16c** bind during the 6 ns, the quinazoline moiety of **14g** presents a constant interaction with adenines (ADE17, ADE18) forming both hydrogen bonds and hydrophobic interactions, while ligand **16c** only interacted with one adenine (ADE5).

Moreover, the interactions of ligand **16c** with EGFR (Fig. 19A), presenting a range between 0.10 and 0.15 nm, mainly to quinazoline moiety forms sustained interactions with residues Val726, Ala743, Leu844, Leu792, and Met1002 for 10 ns.

Moreover, Fig. 19A shows the interaction of **16a** with VEGFR-2 is unstable with wide ranges of variation in the conformation of the structure with peaks at 2, 3, 5 and 8 ns, ranging from 0.10 to 0.45 nm, and this is due to the strong interaction with water, which goes from having four hydrogen bonds in the first 2 ns to having more than six with water molecules after 4 ns, maintaining this trend up to 10 ns. Regarding the frequency of those type of interaction between the ligand **16c** with EGFR shows an almost constant trend into the active site with hydrophobic interactions during the 10 ns (Fig. 19A). Halogenated bond formation is also observed by the 2-chlorine atom of the quinazoline **16c** for both the interaction with EGFR and DNA, which could induce an additive or synergistic effect in antiproliferative activity.[52] Further, the interaction of **16a** into VEGFR-2 receptor, presents the same tendency of hydrogen bond formation but in smaller number in comparison to **16c**-DNA.

3. Conclusions

The anticancer activity of the new series of quinazoline-chalcones **14a–g** and pyrimidodiazepines **16a–g** against 60 cancer cell lines of different panels of human tumor revealed that most of the assayed compounds exhibited significant

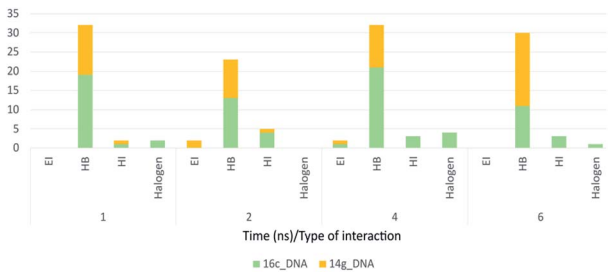

Fig. 18 Frequency of type of interaction between ligand-receptor **14g**-DNA and **16c**-DNA during 6 ns. HI: hydrophobic interactions; HB: hydrogen bonds; EI: electrostatic interactions.

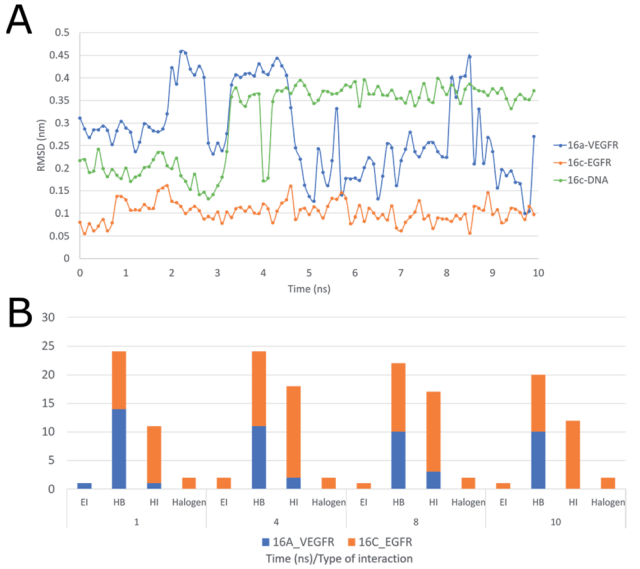

Fig. 19 (A) RMSD of ligand interactions **16a**-VEGFR, **16c**-EGFR, **16c**-DNA. (B) Frequency of type of interactions between ligand-receptor **16c**-EGFR and **16a**-VEGFR during 10 ns, HI: hydrophobic interactions; HB: hydrogen bonds; EI: electrostatic interactions.

growth inhibition percentages and lethality especially compounds **14g**, **16a** and **16c**. The results showed that quinazoline-chalcone **14g** exhibited high antiproliferative activity being effective against leukemia cell line K-562 with a GI_{50} value of 0.622 μM. Compounds **16a** and **16c** showed better cytostatic (TGI) and/or cytotoxic activity (LC_{50}) than adriamycin/doxorubicin against HL-60(TB) (leukemia), HCT-116 (colon cancer), HCT-15 (colon cancer), SW-620 (colon cancer), OVCAR-3 (ovarian cancer), OVCAR-4 (ovarian cancer), ACHN (renal cancer), CAKI-1 (renal cancer), DU-145 (prostate cancer) and MDA-MB-231/ATCC (breast cancer), where compound **16c** showed better LC_{50} values than adriamycin/doxorubicin, being 10.0-fold more active against ten cancer cell lines. DNA binding study has shown that compounds **14g** and **16c** may interact with the DNA strands through groove binding with binding constant (K_b) of 9.3×10^3 and 7.1×10^3 M^{-1}, respectively. These results suggest that compound **14g** has more prominent interaction with DNA than CCNU (lomustine). Molecular docking study was carried out for DNA, EGFR, and VEGFR-2 receptors, showing that the compounds **14g**, **16c** and **16a** have better binding energies of −8.30, −9.90 and −9.20 kcal mol^{-1}, respectively, including mainly hydrogen bonds and hydrophobic interactions. Also, compounds **14g** and **16c** interacted with DNA through intercalation and groove binding, according to binding constant (K_b) and docking results. Finally, the interactions of ligand **16c** with EGFR showed an almost constant trend into the active site with hydrophobic interactions with residues Val726, Ala743, Leu844, Leu792, and Met1002 by molecular dynamics simulation. All these findings may help to understand the possible mechanism of action of those quinazoline derivatives.

4. Experimental section

4.1 General information

Reagents and solvents used were purchased from Sigma-Aldrich. Reactions were monitored by TLC on Merck silica gel 60 F254 aluminum plates. Melting points were measured in open glass capillaries using a Stuart SMP10 melting point apparatus. Attenuated total reflection (ATR)-FTIR spectra were obtained on a Shimadzu IRAffinity-1. ^{1}H and ^{13}C NMR spectra were run on a BRUKER DPX 400 spectrometer operating at 400 and 100 MHz, respectively, using DMSO-d_6 as solvent and tetramethylsilane as internal standard. Mass spectra were obtained on a SHIMADZU-GCMS-QP2010 spectrometer operating at 70 eV. The elemental analyses were performed using a Thermo Finnigan Flash EA1112 CHN (STIUJA) elemental analyzer. The original NMR spectra of representative compounds of series are provided as ESI.†

4.2 Chemistry

4.2.1. Preparation of 1-(3-((2-chloro-6,7-dimethoxyquinazolin-4-yl)amino)phenyl)ethan-1-one (11). A mixture of 2,4-dichloro-6,7-dimethoxyquinazoline **9** (1.1 g, 2.2 eq.) and 3′-aminoacetophenone **10** (1.0 g, 1.0 eq.) in *N*,*N*-dimethylformamide (DMF) (6.0 mL) at room temperature. *N*,*N*-Diisopropylethylamine (DIPEA) (1.3 mL, 2.0 eq.) was slowly added dropwise with stirring over 30 min. Then, the reaction mixture was stirred at room temperature for 24 h. The resulting solid was treated with water (20 mL). The solid thus formed was filtered and washed with a mixture of ethanol : water (6 : 4) to provide the 2-chloro-4-anilinoquinazoline **11** as a white solid, which did not require further purification. White solid; 45% yield; mp 239–241 °C; FTIR (ATR) ν(cm^{-1}): 3447 (N–H), 3082 (=C–H), 1674 (C=O), 1512 and 1433 (C=N and C=C). ^{1}H NMR (400 MHz, DMSO-d_6) δ ppm 9.12 (s, 1H, NH), 7.46 (s, 1H, $H_{Bo'}$), 7.26 (d, J = 7.9 Hz, 1H, H_{Bo}), 7.03 (s, 1H, H-5), 6.93 (d, J = 7.7 Hz, 1H, H_{Bp}), 6.74 (t, J = 7.9 Hz, 1H, H_{Bm}), 6.33 (s, 1H, H-8), 3.12 (s, 3H, OCH_3), 3.09 (s, 3H, OCH_3), 1.78 (s, 3H, $COCH_3$). ^{13}C NMR (100 MHz, DMSO-d_6) δ ppm 197.6, 157.8, 155.1, 154. 0, 149.1, 148.3, 139.1, 137.2, 129.0, 127.0, 124.1, 121.6, 107.3, 106.7, 102.2, 56.3, 56.0, 26.8. MS (EI): m/z 357/359 [M^+/M + 2$^+$] (82/27), 356/358 (66/38), 322 (36), 43 (100). Anal. calcd. For $C_{18}H_{16}ClN_3O_3$: C, 60.43; H, 4.51; N, 11.74. Found: C, 60.52; H, 4.71; N, 11.65.

4.2.2. Preparation of 1,1′-(((6,7-dimethoxyquinazoline-2,4-diyl)bis(azanediyl))bis(3,1-phenylene))bis(ethan-1-one) (12). A mixture of 2,4-dichloro-6,7-dimethoxyquinazoline **9** (1.1 g, 2.2 eq.) and 3′-aminoacetophenone **10** (1.0 g, 1.0 eq.) in ethanol (10.0 mL) was heated under reflux for 4 h and then cooled to room temperature. The resulting solid was filtered and washed with a mixture of ethanol : water (1 : 1) to provide the 4-anilinoquinazoline **12** as a white solid, which did not require further purification. White solid; 63% yield; mp 258–260 °C; FTIR (ATR) ν(cm^{-1}): 3377 (N–H), 3211 (=C–H), 1681 and 1639 (C=O), 1560 and 1479 (C=N and C=C). ^{1}H NMR (400 MHz, DMSO-d_6) δ ppm 10.71 (s, 1H, NH), 8.77 (s, 1H, NH), 8.25–7.99 (m, 3H, 2× $H_{Bo'}$, H-5), 7.75–7.13 (m, 5H, 2× H_{Bo}, 2× H_{Bp}, H_{Bm}), 6.90–6.76

(m, 2H, H_{Bm}, H-8), 3.88 (s, 3H, OCH_3), 3.82 (s, 3H, OCH_3), 2.60 (s, 6H, 2× $COCH_3$). ^{13}C NMR (100 MHz, DMSO-d_6) δ ppm 197.7, 162.4, 161.0, 154.9, 154.8, 150.4, 146.7, 146.3, 145.0, 139.6, 137.4, 136.5, 129.2, 123.6, 122.1, 118.4, 110.7, 107.1, 106.5, 105.5, 97.8, 55.8, 55.6, 26.8. MS (EI): *m*/*z* 456 [M^+] (1.82), 353 (19), 339 (99), 324 (100), 164 (48), 43 (100). Anal. calcd. For $C_{26}H_{24}N_4O_4$: C, 68.41; H, 5.30; N, 12.27. Found: C, 68.59; H, 5.45; N, 12.39.

4.2.3. General procedure for the synthesis of quinazoline-chalcones (14a–g). A mixture of 2-chloro-4-anilinoquinazoline **11** (500 mg, 1.40 mmol), the selected aldehyde **13a–g** (1.54 mmol), and a pellet of KOH in methanol (20.0 mL) was stirred at room temperature for 24 h. The precipitated thus formed was filtered and washed with ethanol and water to obtain compounds **14a–g** as pure yellow solids.

*4.2.3.1. (E)-1-(3-((2-Chloro-6,7-dimethoxyquinazolin-4-yl) amino)phenyl)-3-(4-chlorophenyl)prop-2-en-1-one **(14a)**.* Pale yellow solid; 85% yield; mp 230–232 °C; FTIR (ATR) ν(cm^{-1}): 3304 (N–H), 3030 (=C–H), 1658 (C=O), 1595 and 1577 (C=N and C=C). ^{1}H NMR (400 MHz, DMSO-d_6) δ ppm 10.00 (s, 1H, NH), 8.43 (s, 1H, $H_{Bo'}$), 8.15 (d, J = 8.1 Hz, 1H, H_{Bo}), 8.06–7.84 (m, 5H, Hβ, H-5, H_{Co}, H_{Bp}), 7.78 (d, J = 15.5 Hz, 1H, Hα), 7.63 (t, J = 8.1 Hz, 1H, H_{Bm}), 7.53 (d, J = 8.0 Hz, 2H, H_{Cm}), 7.18 (s, 1H, H-8), 3.97 (s, 3H, OCH_3), 3.93 (s, 3H, OCH_3). ^{13}C NMR (100 MHz, DMSO-d_6) δ ppm 188.8, 157.8, 155.0, 154.1, 149.1, 148.3, 142.7, 139.3, 137.9, 135.2, 133.6, 130.5, 129.1, 128.9, 127.1, 124.4, 122.7, 122.0, 107.3, 106.6, 102.2, 56.3, 56.0. MS (EI): *m*/*z* 479/481/483 [M^+/M + 2^+/M + 4^+] (12/11/1), 478/480/482 (4/6/2), 165 (34), 137 (71), 102 (100). Anal. calcd. For $C_{25}H_{19}Cl_2N_3O_3$: C, 62.51; H, 3.99; N, 8.75. Found: C, 62.64; H, 4.32; N, 8.53.

*4.2.3.2. (E)-3-(4-Bromophenyl)-1-(3-((2-chloro-6,7-dimethoxyquinazolin-4-yl)amino)phenyl)prop-2-en-1-one **(14b)**.* Pale yellow solid; 68% yield; mp 197–199 °C; FTIR (ATR) ν(cm^{-1}): 3305 (N–H), 3018 (=C–H), 1659 (C=O), 1597 and 1573 (C=N and C=C). ^{1}H NMR (400 MHz, DMSO-d_6) δ ppm 10.39 (s, 1H, NH), 8.42 (s, 1H, $H_{Bo'}$), 8.13 (d, J = 8.2 Hz, 1H, H_{Bo}), 8.01–7.91 (m, 2H, H_{Bp}, Hβ), 7.90–7.81 (m, 3H, H-5, H_{Co}), 7.75 (d, J = 15.2 Hz, 1H, Hα), 7.65 (d, J = 8.4 Hz, 2H, H_{Cm}), 7.63 (t, J = 7.8 Hz, 1H, H_{Bm}), 7.15 (s, 1H, H-8), 3.95 (s, 3H, OCH_3), 3.92 (s, 3H, OCH_3). ^{13}C NMR (100 MHz, DMSO-d_6) δ ppm 188.9, 157.9, 155.0, 154.1, 150.4, 149.1, 148.3, 145.0, 142.8, 137.9, 136.6, 131.9, 130.9, 130.8, 129.1, 129.0, 122.8, 121.7, 107.4, 106.7, 102.2, 56.3, 56.0. MS (EI): *m*/*z* 523/525/527 [M^+/M + 2^+/M + 4^+] (12/16/4), 488/490 (2/1), 209/211 (7/6), 102 (100). Anal. calcd. For $C_{25}H_{19}BrClN_3O_3$: C, 57.22; H, 3.65; N, 8.01. Found: C, 57.31; H, 3.58; N, 8.15.

*4.2.3.3. (E)-1-(3-((2-Chloro-6,7-dimethoxyquinazolin-4-yl) amino)phenyl)-3-(4-fluorophenyl)prop-2-en-1-one **(14c)**.* Yellow solid; 51% yield; mp 228–230 °C; FTIR (ATR) ν(cm^{-1}): 3385 (N–H), 3005 (=C–H), 1653 (C=O), 1598 and 1571 (C=N and C=C). ^{1}H NMR (400 MHz, DMSO-d_6) δ ppm 10.00 (s, 1H, NH), 8.43 (s, 1H, $H_{Bo'}$), 8.15 (d, J = 8.1 Hz, 1H, H_{Bo}), 8.07–7.72 (m, 6H, H_{Bp}, Hβ, H-5, H_{Co}, Hα), 7.64 (t, J = 8.1 Hz, 1H, H_{Bm}), 7.32 (t, J = 8.8 Hz, 2H, H_{Co}), 7.18 (s, 1H, H-8), 3.97 (s, 3H, OCH_3), 3.93 (s, 3H, OCH_3). ^{13}C NMR (100 MHz, DMSO-d_6) δ ppm 188.8, 163.4 (d, $^1J_{C-F}$ = 249.0 Hz, C), 157.8, 155.0, 149.1, 143.0, 139.3, 138.0, 131.3, 131.2 (d, $^3J_{C-F}$ = 8.8 Hz, CH), 130.8 (d, $^4J_{C-F}$ = 2.6 Hz, C), 129.0, 127.1, 124.4, 122.0, 121.9, 115.9 (d, $^2J_{C-F}$ = 21.7 Hz, CH), 114.8, 107.3, 106.6, 102.2, 56.3, 56.0. MS (EI): *m*/*z* 463/465 [M^+/M + 2^+] (23/8), 149 (45), 121 (83), 101 (100). Anal. calcd. For $C_{25}H_{19}ClFN_3O_3$: C, 64.73; H, 4.13; N, 9.06. Found: C, 64.83; H, 4.16; N, 9.19.

*4.2.3.4. (E)-3-(Benzo[d][1,3]dioxol-5-yl)-1-(3-((2-chloro-6,7-dimethoxyquinazolin-4-yl)amino)phenyl)prop-2-en-1-one **(14d)**.* Yellow solid; 58% yield; mp 252–254 °C; FTIR (ATR) ν(cm^{-1}): 3358 (N–H), 3097 (=C–H), 1635 (C=O), 1599 and 1579 (C=N and C=C). ^{1}H NMR (400 MHz, DMSO-d_6) δ ppm 10.03 (s, 1H, NH), 8.42 (s, 1H, $H_{Bo'}$), 8.14 (d, J = 7.7 Hz, 1H, H_{Bo}), 8.03–7.57 (m, 5H, H_{Bp}, H-5, Hβ, Hα, H_{Co}), 7.35 (d, J = 7.9 Hz, 1H, $H_{Cm'}$), 7.20 (s, 1H, H-8), 7.01 (d, J = 7.9 Hz, 1H, $H_{Co'}$), 6.12 (s, 2H, O–CH_2–O), 3.98 (s, 3H, OCH_3), 3.94 (s, 3H, OCH_3). ^{13}C NMR (100 MHz, DMSO-d_6) δ ppm 188.6, 157.9, 155.1, 154.1, 149.7, 149.1, 148.3, 148.1, 144.3, 139.2, 138.2, 129.1, 129.0, 127.0, 126.0, 124.4, 122.1, 119.9, 108.6, 107.3, 106.9, 106.7, 102.2, 101.7, 56.3, 56.0. MS (EI): *m*/*z* 222 (40), 207 (17), 136 (42), 43 (100). Anal. calcd. For $C_{26}H_{20}ClN_3O_5$: C, 63.74; H, 4.12; N, 8.58. Found: C, 63.65; H, 4.18; N, 8.63.

*4.2.3.5. (E)-1-(3-((2-Chloro-6,7-dimethoxyquinazolin-4-yl) amino)phenyl)-3-(4-methoxyphenyl)prop-2-en-1-one **(14e)**.* Yellow solid; 56% yield; mp 217–218 °C; FTIR (ATR) ν(cm^{-1}): 3365 (N–H), 3078 (=C–H), 1635 (C=O), 1581 and 1558 (C=N and C=C). ^{1}H NMR (400 MHz, DMSO-d_6) δ ppm 10.18 (s, 1H, NH), 8.40 (s, 1H, $H_{Bo'}$), 8.08 (d, J = 8.8 Hz, 1H, H_{Bo}), 7.96–7.75 (m, 6H, H_{Bp}, Hβ, H_{Co}, H-5, Hα), 7.59 (t, J = 8.4 Hz, 1H, H_{Bm}), 7.13 (s, 1H, H-8), 7.02 (d, J = 8.2 Hz, 2H, H_{Cm}), 3.95 (s, 3H, OCH_3), 3.92 (s, 3H, OCH_3), 3.82 (s, 3H, *p*-OCH_3). ^{13}C NMR (100 MHz, DMSO-d_6) δ ppm 188.8, 161.5, 158.0, 154.8, 154.5, 148.9, 148.2, 144.1, 138.3, 137.2, 130.8, 128.9, 127.3, 127.0, 123.7, 122.2, 119.5, 114.5, 108.0, 106.6, 102.6, 56.2, 56.0, 55.4. MS (EI): *m*/*z* 475/477 [M^+/M + 2^+] (62/21), 446 (15), 440 (13), 161 (70), 133 (100), 118 (52). Anal. calcd. For $C_{26}H_{22}ClN_3O_4$: C, 65.62; H, 4.66; N, 8.83. Found: C, 65.76; H, 4.81; N, 8.75.

*4.2.3.6. (E)-1-(3-((2-Chloro-6,7-dimethoxyquinazolin-4-yl) amino)phenyl)-3-(3,4,5-trimethoxyphenyl)prop-2-en-1-one **(14f)**.* Yellow solid; 61% yield; mp 178–180 °C; FTIR (ATR) ν(cm^{-1}): 3363 (N–H), 3001 (=C–H), 1653 (C=O), 1582 and 1575 (C=N and C=C). ^{1}H NMR (400 MHz, DMSO-d_6) δ ppm 9.87 (s, 1H, NH), 8.33 (s, 1H, $H_{Bo'}$), 8.05 (d, J = 8.1 Hz, 1H, H_{Bo}), 7.93 (d, J = 7.7 Hz, 1H, H_{Bp}), 7.90–7.82 (m, 3H, Hβ, H-5), 7.73 (d, J = 15.5 Hz, 1H, Hα), 7.59 (t, J = 7.9 Hz, 1H, H_{Bm}), 7.23 (s, 2H, H_{Co}), 7.10 (s, 1H, H-8), 3.94 (s, 3H, OCH_3), 3.91 (s, 3H, OCH_3), 3.86 (s, 6H, *m*-OCH_3), 3.72 (s, 3H, *p*-OCH_3). ^{13}C NMR (100 MHz, DMSO-d_6) δ ppm 189.1, 158.1, 154.7, 154.6, 153.1, 150.7, 148.6, 148.1, 144.9, 144.6, 139.8, 138.1, 130.2, 128.9, 127.3, 123.6, 122.3, 121.4, 106.6, 106.5, 102.8, 60.2, 60.1, 56.2, 55.9. MS (EI): *m*/*z* 535/537 [M^+/M + 2^+] (100/35), 520/522 (52/18), 500 (10), 135 (31), 77 (41). Anal. calcd. For $C_{28}H_{26}ClN_3O_6$: C, 62.75; H, 4.89; N, 7.84. Found: C, 62.84; H, 4.93; N, 7.94.

*4.2.3.7. (E)-1-(3-((2-Chloro-6,7-dimethoxyquinazolin-4-yl) amino)phenyl)-3-phenylprop-2-en-1-one **(14g)**.* Yellow solid; 57% yield; mp 156–158 °C; FTIR (ATR) ν(cm^{-1}): 3294 (N–H), 3014 (=C–H), 1653 (C=O), 1591 and 1577 (C=N and C=C). ^{1}H NMR (400 MHz, DMSO-d_6) δ ppm 10.01 (s, 1H, NH), 8.46 (s, 1H, $H_{Bo'}$), 8.14 (d, J = 8.0 Hz, 1H, H_{Bo}), 8.02–7.85 (m, 5H, Hβ, H_{Bp}, H_{Cm}, H-

5), 7.80 (d, J = 15.6 Hz, 1H, Hα), 7.63 (t, J = 7.9 Hz, 1H, H_{Bm}), 7.51–7.42 (m, 3H, H_{Co}, H_{Cp}), 7.17 (s, 1H, H-8), 3.97 (s, 3H, OCH_3), 3.93 (s, 3H, OCH_3). ^{13}C NMR (100 MHz, DMSO-d_6) δ ppm 188.9, 157.9, 155.1, 154.1, 149.1, 148.3, 144.3, 139.3, 138.0, 134.6, 130.7, 129.1, 129.0, 128.9, 127.0, 124.3, 122.0, 121.9, 107.3, 106.7, 102.2, 56.3, 56.0. MS (EI): m/z 445/447 [M^+/M + 2^+] (100/30), 410 (31), 380 (23), 131 (46), 103 (82). Anal. calcd. For $C_{25}H_{20}ClN_3O_3$: C, 67.34; H, 4.52; N, 9.42. Found: C, 67.48; H, 4.61; N, 9.48.

4.2.4. General procedure for the synthesis of pyrimidodiazepine derivatives (16a–g). The selected quinazoline-chalcone **14a–g** (0.38 mmol) and 2,4,5,6-tetraminopyrimidine dihydrochloride 15 (0.42 mmol) in methanol (15.0 mL) were heated under reflux for 10–12 h, and then cooled to room temperature. After water had been added, and the reaction mixture was neutralized with 2 M NH_4OH, and the solid formed was filtered and washed with water. The solid was purified by silica gel column chromatography using dichloromethane/ethanol (10 : 1). These fractions required an additional purification by silica gel column chromatography using ethyl acetate/methanol (10 : 1).

*4.2.4.1. 6-(3-((2-Chloro-6,7-dimethoxyquinazolin-4-yl)amino) phenyl)-8-(4-chlorophenyl)-8,9-dihydro-7H-pyrimido[4,5-b][1,4] diazepine-2,4-diamine (**16a**).* Yellow solid; 58% yield; mp 206–208 °C; FTIR (ATR) ν(cm^{-1}): 3481, 3460, 3371 (N–H), 1568 and 1558 (C=N and C=C). ^{1}H NMR (400 MHz, DMSO-d_6) δ ppm 9.78 (s, 1H, NH), 8.04 (s, 1H, $H_{Bo'}$), 7.85 (s, 1H, H-5), 7.65 (dd, J = 8.0, 1.6 Hz, 1H, H_{Bp}), 7.39–7.25 (m, 2H, H_{Bo}, H_{Bm}), 7.23 (d, J = 8.8 Hz, 2H, H_{Co}), 7.18 (d, J = 8.8 Hz, 2H, H_{Cm}), 7.16 (s, 1H, H-8), 7.09 (d, J = 5.8 Hz, 1H, NH), 6.21 (s, 2H, 4-NH_2), 5.69 (d, J = 3.9 Hz, 2H, 2-NH_2), 5.07 (dt, J = 6.6, 3.9 Hz, 1H, $H_{8'}$), 3.93 (s, 3H, OCH_3), 3.93–3.81 (m, 4H, OCH_3, $H_{7b'}$), 2.82 (dd, J = 14.9, 6.8 Hz, 1H, $H_{7a'}$). ^{13}C NMR (100 MHz, DMSO-d_6) δ ppm 163.7, 160.4, 157.9, 154.9, 154.7, 154.5, 154.3, 153.3, 150.3, 149.0, 148.2, 146.8, 143.0, 141.3, 138.3, 131.1, 128.0, 127.8, 122.0, 120.0, 106.6, 102.4, 101.4, 56.6, 56.3, 56.0, 38.6. MS (EI): m/z 601/603/605 [M^+/M + 2^+/M + 4^+] (2.81/1/1), 577 (6), 551 (5), 43 (100). Anal. calcd. For $C_{29}H_{25}Cl_2N_9O_2$: C, 57.81; H, 4.18; N, 20.92. Found: C, 58.12; H, 4.04; N, 21.20.

*4.2.4.2. 8-(4-Bromophenyl)-6-(3-((2-chloro-6,7-dimethoxyquinazolin-4-yl)amino)phenyl)-8,9-dihydro-7H-pyrimido[4,5-b] [1,4]diazepine-2,4-diamine (**16b**).* Yellow solid; 50% yield; mp 254–255 °C; FTIR (ATR) ν(cm^{-1}): 3473, 3352 (N–H), 1567 and 1554 (C=N and C=C). ^{1}H NMR (400 MHz, DMSO-d_6) δ ppm 9.81 (s, 1H, NH), 8.05 (s, 1H, $H_{Bo'}$), 7.86 (s, 1H, H-5), 7.67 (d, J = 7.7 Hz, 1H, H_{Bp}), 7.40–7.26 (m, 4H, H_{Co}, H_{Bo}, H_{Bm}), 7.19–7.06 (m, 4H, H_{Cm}, H-8, NH), 6.27 (s, 2H, 4-NH_2), 5.75 (s, 2H, 2-NH_2), 5.05 (t, J = 5.8 Hz, 1H, $H_{8'}$), 3.94 (s, 3H, OCH_3), 3.94–3.84 (m, 4H, OCH_3, $H_{7b'}$), 2.83 (dd, J = 14.6, 6.7 Hz, 1H, $H_{7a'}$). ^{13}C NMR (100 MHz, DMSO-d_6) δ ppm 163.7, 160.4, 157.9, 155.0, 154.7, 154.6, 154.3, 153.3, 149.0, 148.4, 148.2, 146.8, 143.4, 141.3, 138.4, 130.9, 128.2, 120.0, 119.7, 107.3, 102.4, 101.4, 56.6, 56.3, 56.0, 39.5, 38.6. MS (EI): m/z 645/647/649 [M^+/M + 2^+/M + 4^+] (1/1.4/0.5), 563 (1), 184 (10), 91 (54), 43 (100). Anal. calcd. For $C_{29}H_{25}BrClN_9O_2$: C, 53.84; H, 3.90; N, 19.49. Found: C, 53.46; H, 3.67; N, 20.01.

*4.2.4.3. 6-(3-((2-Chloro-6,7-dimethoxyquinazolin-4-yl)amino) phenyl)-8-(4-fluorophenyl)-8,9-dihydro-7H-pyrimido[4,5-b][1,4] diazepine-2,4-diamine (**16c**).* Yellow solid; 55% yield; mp 241–242 °C; FTIR (ATR) ν(cm^{-1}): 3483, 3363, 3248 (N–H), 1564 and 1554 (C=N and C=C). ^{1}H NMR (400 MHz, DMSO-d_6) δ ppm 9.83 (s, 1H, NH), 8.08 (s, 1H, $H_{Bo'}$), 7.88 (s, 1H, H-5), 7.66 (d, J = 7.5 Hz, 1H, H_{Bp}), 7.36–7.26 (m, 2H, H_{Bo}, H_{Bm}), 7.21 (dd, J = 8.4, $^4J_{H-F}$ = 5.5 Hz, 2H, H_{Co}), 7.16 (s, 1H, H-8), 7.11 (d, J = 5.7 Hz, 1H, NH), 7.00 (t, J = 8.7 Hz, 2H, H_{Cm}), 6.29 (s, 2H, 4-NH_2), 5.76 (s, 2H, 2-NH_2), 5.06 (t, J = 6.2 Hz, 1H, $H_{8'}$), 3.95 (s, 3H, OCH_3), 3.92 (s, 3H, OCH_3), 3.83 (dd, J = 14.9, 6.0 Hz, 1H, $H_{7b'}$), 2.85 (dd, J = 14.9, 6.8 Hz, 1H, $H_{7a'}$). ^{13}C NMR (100 MHz, DMSO-d_6) δ ppm 163.6, 162.3, 160.9 (d, $^1J_{C-F}$ = 242.5 Hz, C), 157.9, 155.0, 154.6, 154.3, 153.6, 148.2, 141.3, 140.2, 138.3, 128.2, 127.8 (d, $^3J_{C-F}$ = 7.5 Hz, CH), 122.5, 122.1 (d, $^4J_{C-F}$ = 3.2 Hz, C), 120.1, 114.7 (d, $^2J_{C-F}$ = 21.4 Hz, CH), 107.3, 106.7, 102.4, 101.3, 56.7, 56.3, 56.0, 38.7. MS (EI): m/z 406 (2), 264 (2), 149 (13), 57 (60), 43 (100). Anal. calcd. For $C_{29}H_{25}ClFN_9O_2$: C, 59.44; H, 4.30; N, 21.51. Found: C, 60.11; H, 4.29; N, 21.47.

*4.2.4.4. 8-(Benzo[d][1,3]dioxol-5-yl)-6-(3-((2-chloro-6,7-dimethoxyquinazolin-4-yl)amino)phenyl)-8,9-dihydro-7H-pyrimido[4,5-b][1,4]diazepine-2,4-diamine (**16d**).* Yellow solid; 56% yield; mp 233–235 °C; FTIR (ATR) ν(cm^{-1}): 3483, 3353 (N–H), 1568 and 1554 (C=N and C=C). ^{1}H NMR (400 MHz, DMSO-d_6) δ ppm 9.83 (s, 1H, NH), 8.30 (s, 1H, $H_{Bo'}$), 7.87 (s, 1H, H-5), 7.68 (dd, J = 7.7, 2.4 Hz, 1H, H_{Bp}), 7.40 (d, J = 8.0 Hz, 1H, H_{Bo}), 7.32 (t, J = 7.9 Hz, 1H, H_{Bm}), 7.16 (s, 1H, H-8), 6.97 (d, J = 5.4 Hz, 1H, NH), 6.74 (d, J = 1.7 Hz, 1H, H_{Co}), 6.72 (d, J = 8.0 Hz, 1H, $H_{Cm'}$), 6.65 (dd, J = 8.1, 1.8 Hz, 1H, $H_{Co'}$), 6.27 (s, 2H, 4-NH_2), 5.85 (d, J = 10.9 Hz, 2H, O–CH_2–O), 5.73 (s, 2H, 2-NH_2), 4.96 (td, J = 5.9, 2.1 Hz, 1H, $H_{8'}$), 3.95 (s, 3H, OCH_3), 3.92 (s, 3H, OCH_3), 3.72 (dd, J = 14.7, 6.3 Hz, 1H, $H_{7b'}$), 2.86 (dd, J = 14.7, 2.2 Hz, 1H, $H_{7a'}$). ^{13}C NMR (100 MHz, DMSO-d_6) δ ppm 163.6, 160.3, 157.9, 154.9, 154.6, 154.3, 153.7, 149.0, 148.4, 148.2, 147.0, 145.8, 141.4, 138.3, 138.2, 128.2, 122.4, 122.1, 120.1, 119.0, 107.8, 107.3, 106.5, 102.3, 101.3, 100.7, 57.1, 56.3, 56.0, 38.9. MS (EI): m/z 611/613 [M^+/M + 2^+] (1/0.6), 527 (1), 148 (31), 89 (30), 50 (100). Anal. calcd. For $C_{30}H_{26}ClN_9O_4$: C, 58.87; H, 4.28; N, 20.60. Found: C, 59.07; H, 4.13; N, 21.08.

*4.2.4.5. 6-(3-((2-Chloro-6,7-dimethoxyquinazolin-4-yl)amino) phenyl)-8-(4-methoxyphenyl)-8,9-dihydro-7H-pyrimido[4,5-b][1,4] diazepine-2,4-diamine (**16e**).* Yellow solid; 51% yield; mp 208–210 °C; FTIR (ATR) ν(cm^{-1}): 3473, 3371, 3352 (N–H), 1565 and 1554 (C=N and C=C). ^{1}H NMR (400 MHz, DMSO-d_6) δ ppm 9.80 (s, 1H, NH), 8.04 (s, 1H, $H_{Bo'}$), 7.86 (s, 1H, H-5), 7.65 (d, J = 7.9 Hz, 1H, H_{Bp}), 7.38 (d, J = 8.1 Hz, 1H, H_{Bo}), 7.30 (t, J = 7.9 Hz, 1H, H_{Bm}), 7.17 (s, 1H, H-8), 7.10 (d, J = 8.8 Hz, 2H, H_{Co}), 6.97 (d, J = 5.4 Hz, 1H, NH), 6.74 (d, J = 8.8 Hz, 2H, H_{Cm}), 6.25 (s, 2H, 4-NH_2), 5.72 (s, 2H, 2-NH_2), 4.97 (t, J = 5.7 Hz, 1H, $H_{8'}$), 3.95 (s, 3H, OCH_3), 3.93 (s, 3H, OCH_3), 3.73 (dd, J = 14.9, 6.3 Hz, 1H, $H_{7b'}$), 3.61 (s, 3H, p-OCH_3), 2.87 (dd, J = 14.9, 5.4 Hz, 1H, $H_{7a'}$). ^{13}C NMR (100 MHz, DMSO-d_6) δ ppm 163.6, 160.3, 157.9, 157.9, 155.0, 154.7, 154.3, 153.6, 149.0, 148.2, 141.5, 138.3, 136.2, 128.2, 127.0, 122.4, 122.1, 120.1, 113.4, 107.3, 106.7, 102.3, 101.3, 56.6, 56.3, 56.0, 54.9, 38.9. MS (EI): m/z 597/599 [M^+/M + 2^+] (6/2), 577 (6), 578 (6), 458 (7), 134 (100), 91 (64), 44 (83). Anal.

calcd. For $C_{30}H_{28}ClN_9O_3$: C, 60.25; H, 4.72; N, 21.08. Found: C, 60.51; H, 4.19; N, 21.24.

*4.2.4.6. 6-(3-((2-Chloro-6,7-dimethoxyquinazolin-4-yl)amino) phenyl)-8-(3,4,5-trimethoxyphenyl)-8,9-dihydro-7H-pyrimido[4,5-b][1,4]diazepine-2,4-diamine (**16f**).* Yellow solid; 53% yield; mp 203–205 °C; FTIR (ATR) ν(cm^{-1}): 3462, 3379, 3363 (N–H), 1571 and 1554 (C=N and C=C). ^{1}H NMR (400 MHz, DMSO-d_6) δ ppm 9.82 (s, 1H, NH), 8.06 (s, 1H, $H_{Bo'}$), 7.86 (s, 1H, H-5), 7.66 (d, J = 8.0 Hz, 1H, H_{Bp}), 7.50 (d, J = 7.9 Hz, 1H, H_{Bo}), 7.34 (t, J = 6.8 Hz, 1H, H_{Bm}), 7.17 (s, 1H, H-8), 6.93 (d, J = 5.1 Hz, 1H, NH), 6.51 (s, 1H, H_{Co}), 6.24 (s, 2H, 4-NH_2), 5.72 (s, 2H, 2-NH_2), 4.94 (t, J = 5.7 Hz, 1H, $H_{8'}$), 3.94 (s, 3H, OCH_3), 3.88 (s, 3H, OCH_3), 3.78 (dd, J = 14.5, 6.8 Hz, 1H, $H_{7b'}$), 3.57 (s, 6H, *m*-OCH_3), 3.50 (s, 3H, *p*-OCH_3), 2.89 (dd, J = 14.5, 3.8 Hz, 1H, $H_{7a'}$). ^{13}C NMR (100 MHz, DMSO-d_6) δ ppm 163.5, 161.4, 158.6, 157.9, 157.1, 155.0, 154.4, 154.3, 152.5, 149.0, 148.2, 146.8, 141.4, 139.5, 138.3, 136.3, 128.1, 128.0, 122.2, 107.3, 106.7, 103.7, 102.4, 101.4, 56.4, 56.2, 56.0, 55.7, 38.9. MS (EI): m/z 657/659 [M^+/M + 2^+] (3/1), 653 (7), 435 (19), 241 (34), 194 (81), 179 (64), 43 (100). Anal. calcd. For $C_{32}H_{32}ClN_9O_5$: C, 58.40; H, 4.90; N, 19.16. Found: C, 58.65; H, 4.86; N, 19.42.

*4.2.4.7. 6-(3-((2-Chloro-6,7-dimethoxyquinazolin-4-yl)amino) phenyl)-8-phenyl-8,9-dihydro-7H-pyrimido[4,5-b][1,4]diazepine-2,4-diamine (**16g**).* Yellow solid; 50% yield; mp 238–240 °C; FTIR (ATR) ν(cm^{-1}): 3473, 3371, 3311 (N–H), 1568 and 1554 (C=N and C=C). ^{1}H NMR (400 MHz, DMSO-d_6) δ ppm 9.80 (s, 1H, NH), 8.05 (s, 1H, $H_{Bo'}$), 7.86 (s, 1H, H-5), 7.65 (d, J = 7.7 Hz, 1H, H_{Bp}), 7.34 (d, J = 7.9 Hz, 1H, H_{Bo}), 7.28 (t, J = 7.9 Hz, 1H, H_{Bm}), 7.22–7.17 (m, 4H, H_{Co}, H_{Cm}), 7.16 (s, 1H, H-8), 7.12–7.02 (m, 2H, H_{Cp}, NH), 6.27 (s, 2H, 4-NH_2), 5.75 (s, 2H, 2-NH_2), 5.05 (t, J = 5.9 Hz, 1H, $H_{8'}$), 3.94 (s, 3H, OCH_3), 3.92 (s, 3H, OCH_3), 3.81 (dd, J = 14.7, 6.3 Hz, 1H, $H_{7b'}$), 2.86 (d, J = 14.5, 2.1 Hz, 1H, $H_{7a'}$). ^{13}C NMR (100 MHz, DMSO-d_6) δ ppm 163.6, 160.3, 157.9, 154.9, 154.7, 154.3, 153.6, 149.0, 148.2, 144.0, 141.4, 138.3, 128.1, 128.0, 126.7, 125.9, 122.4, 122.1, 120.0, 107.3, 106.6, 102.4, 101.3, 57.2, 56.3, 56.0, 38.9. MS (EI): m/z 567/569 [M^+/M + 2^+] (1/0.2), 551 (1), 73 (100), 44 (76). Anal. calcd. For $C_{29}H_{26}ClN_9O_2$: C, 61.32; H, 4.61; N, 22.19. Found: C, 61.49; H, 4.52; N, 22.27.

4.3 Anticancer activity

The human cancer cell lines of the cancer screening panel were grown in an RPMI-1640 medium containing 5% fetal bovine serum and 2 mM L-glutamine. For a typical screening experiment, cells were inoculated into 96-well microtiter plates. After cell inoculation, the microtiter plates were incubated at 37 °C, 5% CO_2, 95% air, and 100% relative humidity for 24 h prior to the addition of the tested compounds. After 24 h, two plates of each cell line were fixed *in situ* with TCA, to represent a measurement of the cell population for each cell line at the time of sample addition (T_z). The samples were solubilized in dimethyl sulfoxide (DMSO) at 400-fold the desired final maximum test concentration and stored frozen prior to use. At the time of compound addition, an aliquot of frozen concentrate was thawed and diluted to twice the desired final maximum test concentration with complete medium containing 50 μg mL^{-1} gentamicin. An additional four 10-fold or 1/2 log serial dilutions were made to provide a total of five drug concentrations plus the control. Aliquots of 100 μL of these different sample dilutions were added to the appropriate microtiter wells already containing 100 μL of medium, resulting in the required final sample concentrations.[53] After the tested compounds were added, the plates were incubated for an additional 48 h at 37 °C, 5% CO_2, 95% air, and 100% relative humidity. For adherent cells, the assay was terminated by the addition of cold TCA. Cells were fixed *in situ* by the gentle addition of 50 μL of cold 50% (w/v) TCA (final concentration, 10% TCA) and incubated for 60 min at 4 °C. The supernatant was discarded, and plates were washed five times with tap water and air dried. Sulforhodamine B (SRB) solution (100 μL) at 0.4% (w/v) in 1% acetic acid was added to each well, and plates were incubated for 10 min at room temperature. After staining, unbound dye was removed by washing five times with 1% acetic acid and the plates were air dried. Bound stain was subsequently solubilized with 10 mM Trizma base, and the absorbance was read on an automated plate reader at a wavelength of 515 nm. Using the seven absorbance measurements [time zero (T_z), control growth in the absence of drug (C), and test growth in the presence of drug at the five concentration levels (T_i)], the percentage growth was calculated at each of the drug concentrations levels. Percentage growth inhibition was calculated as: $[(T_i - T_z)/(C - T_z)] \times 100$ for concentrations for which $T_i > T_z$, and $[(T_i - T_z)/T_z] \times 100$ for concentrations for which $T_i < T_z$. Two dose–response parameters were calculated for each compound. Growth inhibition of 50% (GI_{50}) was calculated from $[(T_i - T_z)/(C - T_z)] \times 100 = 50$, which is the drug concentration resulting in a 50% lower net protein increase in the treated cells (measured by SRB staining) as compared to the net protein increase seen in the control cells and the LC_{50} (concentration of drug resulting in a 50% reduction in the measured protein at the end of the drug treatment as compared to that at the beginning), indicating a net loss of cells; calculated from $[(T_i - T_z)/T_z] \times 100 = -50$. Values were calculated for each of these two parameters if the level of activity is reached; however, if the effect was not reached or was exceeded, the value for that parameter was expressed as greater or less than the maximum or minimum concentration tested.[53–55]

4.4 Hemolytic activity

The ability to induce hemolysis was evaluated to compounds that showed anticancer activity following the method of cytotoxicity by spectrophotometry. The method was adapted from Conceição *et al.*[56] with modifications. Briefly, 240 μL of human red blood cells (huRBC) adjusted to 5% hematocrit in phosphate buffer saline (PBS) were placed into each well of 96-well plate and subsequently exposed to 200 μg mL^{-1} of the selected compounds (*i.e.*, 10 μL of 5 mg mL^{-1} working solution of each compound in MHB with 5% DMSO 0.1% Tween-80). As positive control for hemolytic activity 10 μL SDS 1% was added. For a negative control only medium with no chemicals was added to huRBC. Free hemoglobin was measured after 24 h incubation at 37 °C by spectrophotometry (420 nm Cytation 3M, BioteK). Non-specific absorbance was subtracted from a blank.

Determinations were done by triplicate in at least two independent experiments.

4.5 DNA binding study

The binding properties of the compounds **14g** and **16c** with highly polymerized and lyophilized calf thymus DNA (ctDNA, type I, fibers, Sigma-Aldrich, Lot#SLBJ8916V PCode 1001817527) have been studied using electronic absorption experiments and viscosity measurements, following standard methodologies and procedures previously adopted by our laboratory.[57] Stock solutions of ctDNA were prepared using a solution of Tris (10 mM) and EDTA (1 mM) in deionized water (pH = 7.5) and stored at −5 °C. Concentration was determined spectrophotometrically at 25 °C, using ε_{260} = 6600 L cm^{-1} mol^{-1} as molar extinction coefficient and measuring the absorbance at 260 nm. The purity of ctDNA was determined by monitoring the absorbance ratio at 260 nm to that at 280 nm. The observed A_{260}/A_{280} ratio between 1.7 and 1.9 for ctDNA solutions indicates that the DNA was free of RNA and proteins.

4.5.1. UV-vis spectroscopy studies. The electronic absorption spectra were recorded in an UV-visible Evolution 220 Thermo Scientific spectrophotometer, equipped with Single Cell Peltier System for temperature control. The binding experiments were carried at fixed concentration of 70 μM and 60 μM for compounds **14g** and **16c** respectively, and increasing ctDNA concentration (0–96 μM) at 25 °C. The use of multiple concentrations of the compounds examined in the study allowed the acquisition of clear and reliable absorbance values in optimal ranges for quantification (0.7–1.2 AU) and achieved DNA saturation when adding small amounts of the compound, allowing dilution effects to be avoided. After each addition of titrant, the electronic absorption spectra of the evaluated compound were measured in the wavelength range of 230–750 nm. The ctDNA absorbance was eliminated by adding an equal amount of ctDNA to the sample and the reference solution.[58]

4.5.2. DNA melting measurements. Melting curves for ctDNA were obtained from measurements of ctDNA absorbance at 260 nm in the absence and presence of compounds at the same concentration (80 μM) using the Peltier accessory at 20–80 °C, at intervals of 5 °C. The denaturation temperature (T_m) of ctDNA was evaluated following the recommended procedure.[46]

4.5.3. Viscosity measurements. The relative viscosities of solutions containing ctDNA at a constant concentration (500 μM) and five increasing concentrations of the study compounds (150–750 μM) were determined. A Semi-Micro Cannon-Ubbelohde viscometer 75 was used at a controlled temperature in a thermal bath maintained at 22 °C. Viscosities were calculated based on the relationship between the kinetic viscosities of the ctDNA–compound mixtures and that of free DNA, which was calculated using the viscometer constant and the flow times.

4.6 Molecular docking

4.6.1. Construction of the ligands 3D model and preparation for docking. The 2D structure of the ligands **14g**, **16a**, **16c** were plotted in Chemdraw online version (https://chemdrawdirect.perkinelmer.cloud/js/sample/index.html). The Avogadro version 1.2 software was used (https://avogadro.cc/) to convert the ligands to 3D model and were optimized with the steepest descent algorithm using the Universal Force Field (UFF).[59] The 3D structures of the positive controls (interaction with receptors experimentally validated) were downloaded in PDB format from the Drugbank (https://go.drugbank.com/). DNA intercalant agent mitoxantrone[48,49] was used for interaction with DNA (1BNA). Two controls were taken for both EGFR (gefitinib and lapatinib) and VEGFR-2 (sorafenib and tivozanib) receptors. The structures of the ligands and controls were prepared with Autodock software[50] using Gasteiger charges.[51]

4.6.2. Preparation of DNA, EGFR, and VEGFR-2 receptors for docking. EGFR (PDB: 1XKK) and VEGFR-2 (PDB: 4ASE) receptors were selected according to previous work by Allam *et al.*[1] and Barbosa *et al.*,[13] respectively. Target receptor (PDBID: 1BNA, sequence d(CGCGAATTCGCG)2) was used because represents the best B-DNA structure due to its high resolution of 1.90 Å with a tendency to double symmetry in the conformation of the sugars around the center of the molecule.[60] The 1BNA structure is highly used in molecular docking for testing effects on DNA with anticancer ligands in papers such as those of Gul *et al.*,[61] Rezki *et al.*,[62] and Singh *et al.*[63] The pymol software (https://pymol.org/2/) was used to remove water molecules and other ligands within each receptor. The proteins preparation were performed using Autodock software[50] with addition of Kollman charges and optimization of the hydrogen bond (H-bond). The coordinates of grid were obtained from each molecule present in the PDBs of the receptors, and the grid box was confirmed with the CB-Dock (blind docking) online tool (http://cao.labshare.cn/cb-dock/) using the prepared ligands and protein.

4.6.3. Molecular docking analysis. The conformer with minimum binding energy was picked up from the one minimum energy (root mean square deviation, RMSD = 0.0) conformers from the 50 runs using Autodock. Discovery Studio Visualizer software (http://accelrys.com) was used to analyze ligand-receptor interactions to find the amino acids that interact with the molecules.

4.7 Molecular dynamics simulation and analysis

Molecular dynamic simulations were performed with NAMD software version 2.14.[64] The concentration of KCl was 0.15 M as determined by the Monte Carlo method, with water thickness of 22.5 Å and CHARMM36m as a force field.[65] The systems were adjusted by slowly heating to a temperature of 310 K at 2 fs (femtosecond) per step for 75 ps (picoseconds). For equilibration 90 000 000 numsteps were used. Once the system is equilibrated at the desired temperature and pressure MD was ran for data collection for 10 ns. We used pymol for extract the molecules PDB at 1, 4, 8 and 10 ns and Discovery studio for the analysis of interactions.

Author contributions

Viviana Cuartas: methodology, experimental details, and writing original draft. Alberto Aragón-Muriel: methodology and

experimental details. Yamil Liscano: experimental details, formal analysis and writing original draft. Dorian Polo-Cerón: conceptualization, resources, and writing – review & editing. Maria P. Crespo-Ortiz: experimental details. Jairo Quiroga: conceptualization and funding acquisition. Rodrigo Abonia: resources, funding acquisition. Braulio Insuasty: conceptualization, supervision, and writing – review & editing.

Conflicts of interest

There are no conflicts to declare.

Acknowledgements

The authors would like to thank the U.S. National Cancer Institute (NCI), for *in vitro* anticancer screening of the compounds. This research was supported by the Universidad del Valle, Universidad Santiago de Cali, MINCIENCIAS (110680864255) and the Science, Technology and Innovation Fund-General Royalties System (FCTeI-SGR) under contract BPIN 2013000100007.

References

1 H. A. Allam, E. E. Aly, A. K. B. A. W. Farouk, A. M. El Kerdawy, E. Rashwan and S. E. S. Abbass, *Bioorg. Chem.*, 2020, **98**, 103726.
2 M. D. Canela, S. Noppen, O. Bueno, A. E. Prota, K. Bargsten, G. Sáez-Calvo, M. L. Jimeno, M. Benkheil, D. Ribatti, S. Velázquez, M. J. Camarasa, J. Fernando Díaz, M. O. Steinmetz, E. M. Priego, M. J. Pérez-Pérez and S. Liekens, *Oncotarget*, 2017, **8**, 14325–14342.
3 WHO, Cancer, https://www.who.int/health-topics/cancer#tab=tab_1.
4 B. Mansoori, A. Mohammadi, S. Davudian, S. Shirjang and B. Baradaran, *Adv. Pharm. Bull.*, 2017, **7**, 339–348.
5 M. Sun, J. Jia, H. Sun and F. Wang, *Bioorg. Med. Chem. Lett.*, 2020, **30**, 127045.
6 Y. Li, J. Xiao, Q. Zhang, W. Yu, M. Liu, Y. Guo, J. He and Y. Liu, *Bioorg. Med. Chem.*, 2019, **27**, 568–577.
7 S. A. Elmetwally, K. F. Saied, I. H. Eissa and E. B. Elkaeed, *Bioorg. Chem.*, 2019, **88**, 102944.
8 G. Verma, M. F. Khan, W. Akhtar, M. M. Alam, M. Akhter, O. Alam, S. M. Hasan and M. Shaquiquzzaman, *Arabian J. Chem.*, 2019, **12**, 4815–4839.
9 N. Fayyazi, A. Fassihi, S. Esmaeili, S. Taheri, J. B. Ghasemi and L. Saghaie, *Int. J. Biol. Macromol.*, 2020, **142**, 94–113.
10 M. T. Conconi, G. Marzaro, L. Urbani, I. Zanusso, R. Di Liddo, I. Castagliuolo, P. Brun, F. Tonus, A. Ferrarese, A. Guiotto and A. Chilin, *Eur. J. Med. Chem.*, 2013, **67**, 373–383.
11 H. Q. Zhang, F. H. Gong, C. G. Li, C. Zhang, Y. J. Wang, Y. G. Xu and L. P. Sun, *Eur. J. Med. Chem.*, 2016, **109**, 371–379.
12 K. Abouzid and S. Shouman, *Bioorg. Med. Chem.*, 2008, **16**, 7543–7551.
13 M. L. D. C. Barbosa, L. M. Lima, R. Tesch, C. M. R. Sant'Anna, F. Totzke, M. H. G. Kubbutat, C. Schächtele, S. A. Laufer and E. J. Barreiro, *Eur. J. Med. Chem.*, 2014, **71**, 1–14.
14 K. El-Adl, M. K. Ibrahim, M. S. I. Alesawy and I. H. Eissa, *Bioorg. Med. Chem.*, 2021, **30**, 115958.
15 A. Garofalo, L. Goossens, B. Baldeyrou, A. Lemoine, S. Ravez, P. Six, M. H. David-Cordonnier, J. P. Bonte, P. Depreux, A. Lansiaux and J. F. Goossens, *J. Med. Chem.*, 2010, **53**, 8089–8103.
16 M. U. Rahman, G. Jeyabalan, P. Saraswat, G. Parveen, S. Khan and M. S. Yar, *Synth. Commun.*, 2017, **47**, 379–408.
17 J. M. de la Torre, M. Nogueras and J. Cobo, *Arabian J. Chem.*, 2019, **12**, 4579–4595.
18 D. Verma, P. Kumar, B. Narasimhan, K. Ramasamy, V. Mani, R. K. Mishra and A. B. A. Majeed, *Arabian J. Chem.*, 2019, **12**, 2882–2896.
19 D. Huang, L. Huang, Q. Zhang and J. Li, *Eur. J. Med. Chem.*, 2017, **140**, 212–228.
20 G. Li, X. Wang, C. Tian, T. Zhang, Z. Zhang and J. Liu, *Tetrahedron Lett.*, 2012, **53**, 5193–5196.
21 M. Melguizo, A. Sánchez, M. Nogueras, J. N. Low, R. Alan Howie, G. Andrei and E. De Clercq, *Tetrahedron*, 1994, **50**, 13511–13522.
22 Q. Zhang, Q. Shen, L. Gao, L. Tong, J. Li, Y. Chen and W. Lu, *Eur. J. Med. Chem.*, 2018, **158**, 428–441.
23 S. Xu, L. Zhang, S. Chang, J. Luo, X. Lu, Z. Tu, Y. Liu, Z. Zhang, Y. Xu, X. Ren and K. Ding, *MedChemComm*, 2012, **3**, 1155–1159.
24 J. Ramírez, L. Svetaz, J. Quiroga, R. Abonia, M. Raimondi, S. Zacchino and B. Insuasty, *Eur. J. Med. Chem.*, 2015, **92**, 866–875.
25 F. Liu, X. Chen, A. Allali-Hassani, A. M. Quinn, G. A. Wasney, A. Dong, D. Barsyte, I. Kozieradzki, G. Senisterra, I. Chau, A. Siarheyeva, D. B. Kireev, A. Jadhav, J. M. Herold, S. V. Frye, C. H. Arrowsmith, P. J. Brown, A. Simeonov, M. Vedadi and J. Jin, *J. Med. Chem.*, 2009, **52**, 7950–7953.
26 B. Insuasty, A. García, J. Bueno, J. Quiroga, R. Abonia and A. Ortiz, *Arch. Pharm.*, 2012, **345**, 739–744.
27 B. Insuasty, A. García, J. Quiroga, R. Abonia, M. Nogueras and J. Cobo, *Eur. J. Med. Chem.*, 2010, **45**, 2841–2846.
28 National Cancer Institute, NCI-60 Screening Methodology, https://dtp.cancer.gov/discovery_development/nci-60/methodology.htm.
29 M. R. Boyd and K. D. Paull, *Drug Dev. Res.*, 1995, **34**, 91–109.
30 R. H. Shoemaker, *Nat. Rev. Cancer*, 2006, **6**, 813–823.
31 D. W. Zaharevitz, S. L. Holbeck, C. Bowerman and P. A. Svetlik, *J. Mol. Graphics Modell.*, 2002, **20**, 297–303.
32 G. Berger, H. Leclercqz, A. Derenne, M. Gelbcke, E. Goormaghtigh, J. Nève, V. Mathieu and F. Dufrasne, *Bioorg. Med. Chem.*, 2014, **22**, 3527–3536.
33 D. Havrylyuk, B. Zimenkovsky, O. Vasylenko, C. W. Day, D. Smee, P. Grellier and R. Lesyk, *Eur. J. Med. Chem.*, 2013, **66**, 228–237.
34 M. H. El-Wakil, A. F. El-Yazbi, H. M. A. Ashour, M. A. Khalil, K. A. Ismail and I. M. Labouta, *Bioorg. Chem.*, 2019, **90**, 103089.

35 H. N. Jayaram, M. S. Lui, J. Plowman, K. Pillwein, M. A. Reardon, W. L. Elliott and G. Weber, *Cancer Chemother. Pharmacol.*, 1990, **26**, 88–92.
36 D. A. Skoufias, S. DeBonis, Y. Saoudi, L. Lebeau, I. Crevel, R. Cross, R. H. Wade, D. Hackney and F. Kozielski, *J. Biol. Chem.*, 2006, **281**, 17559–17569.
37 L. H. Li, L. G. Timmins, T. L. Wallace, W. C. Krueger, M. D. Prairie and W. B. Im, *Cancer Lett.*, 1984, **23**, 279–288.
38 National Cancer Institute, CCNU, https://www.cancer.gov/espanol/publicaciones/diccionarios/diccionario-cancer/def/ccnu.
39 E. Movahedi, A. R. Rezvani and H. Razmazma, *Int. J. Biol. Macromol.*, 2019, **126**, 1244–1254.
40 R. G. Shinde, A. A. Khan and A. Barik, *J. Mol. Struct.*, 2020, **1208**, 127901.
41 E. S. Gil, C. B. da Silva, P. A. Nogara, C. H. da Silveira, J. B. T. da Rocha, B. A. Iglesias, D. S. Lüdtke, P. F. B. Gonçalves and F. S. Rodembusch, *J. Mol. Liq.*, 2020, **297**, 111938.
42 T. Biver, *Appl. Spectrosc. Rev.*, 2012, **47**, 272–325.
43 N. Vamsikrishna, S. Daravath, N. Ganji, N. Pasha and K. Shivaraj, *Inorg. Chem. Commun.*, 2020, **113**, 107767.
44 S. Bi, X. Sun, X. Li, R. Zhao and D. Shao, *Luminescence*, 2020, **35**, 493–502.
45 S. Agarwal, D. Chadha and R. Mehrotra, *J. Biomol. Struct. Dyn.*, 2015, **33**, 1653–1668.
46 M. Dareini, Z. Amiri Tehranizadeh, N. Marjani, R. Taheri, S. Aslani-Firoozabadi, A. Talebi, N. NayebZadeh Eidgahi, M. R. Saberi and J. Chamani, *Spectrochim. Acta, Part A*, 2020, **228**, 117528.
47 Y. Ma, G. Zhang and J. Pan, *J. Agric. Food Chem.*, 2012, **60**, 10867–10875.
48 N. L. Huang and J. H. Lin, *Molecules*, 2014, **19**, 7415–7428.
49 D. E. Arthur, *Radiol. Infect. Dis.*, 2019, **6**, 68–79.
50 O. Trott and A. J. Olson, *J. Comput. Chem.*, 2010, **31**, 455–461.
51 J. Gasteiger and M. Marsili, *Tetrahedron Lett.*, 1978, **19**, 3181–3184.
52 J. Schmitt, E. Goodfellow, S. Huang, C. Williams, I. N. F. Gomes, M. N. Rosa, R. M. Reis, R. Yang, H. M. Titi and B. J. Jean-Claude, *Eur. J. Med. Chem.*, 2020, **192**, 112185.
53 A. Monks, D. Scudiero, P. Skehan, R. Shoemaker, K. Paull, D. Vistica, C. Hose, J. Langley, P. Cronise, A. Vaigro-wolff, M. Gray-goodrich, H. Campbell, J. Mayo and M. Boyd, *J. Natl. Cancer Inst.*, 1991, **83**, 757–766.
54 J. N. Weinstein, T. G. Myers, P. M. O'Connor, S. H. Friend, A. J. Fornace, K. W. Kohn, T. Fojo, S. E. Bates, L. V. Rubinstein, N. L. Anderson, J. K. Buolamwini, W. W. van Osdol, A. P. Monks, D. A. Scudiero, E. A. Sausville, D. W. Zaharevitz, B. Bunow, V. N. Viswanadhan, G. S. Johnson, R. E. Wittes and K. D. Paull, *Science*, 1997, **275**, 343–349.
55 M. R. Grever, S. A. Schepartz and B. A. Chabner, *Semin. Oncol.*, 1992, **19**, 622–638.
56 K. Conceição, K. Konno, M. Richardson, M. M. Antoniazzi, C. Jared, S. Daffre, A. C. M. Camargo and D. C. Pimenta, *Peptides*, 2006, **27**, 3092–3099.
57 J. D. Londoño-Mosquera, A. Aragón-Muriel and D. Polo-Cerón, *Univ. Sci.*, 2018, **23**, 141–169.
58 H. L. Chen, P. Y. Su, Y. S. Chang, S. Y. Wu, Y. Di Liao, H. M. Yu, T. L. Lauderdale, K. Chang and C. Shih, *PLoS Pathog.*, 2013, **9**, e1003425.
59 A. K. Rappe, C. J. Casewit, K. S. Colwell, W. A. Goddard and W. M. Skiff, *J. Am. Chem. Soc.*, 1992, **114**, 10024–10035.
60 H. R. Drew, R. M. Wing, T. Takano, C. Broka, S. Tanaka, K. Itakura and R. E. Dickerson, *Proc. Natl. Acad. Sci. U. S. A.*, 1981, **78**, 2179–2183.
61 A. Gul, Z. Akhter, F. Perveen, S. Kalsoom, F. L. Ansari and M. Siddiq, *Int. J. Polym. Sci.*, 2019, **2019**, 2103891.
62 N. Rezki, F. F. Al-Blewi, S. A. Al-Sodies, A. K. Alnuzha, M. Messali, I. Ali and M. R. Aouad, *ACS Omega*, 2020, **5**, 4807–4815.
63 I. Singh, V. Luxami and K. Paul, *Sci. Rep.*, 2020, **10**, 6534.
64 J. C. Phillips, D. J. Hardy, J. D. C. Maia, J. E. Stone, J. V. Ribeiro, R. C. Bernardi, R. Buch, G. Fiorin, J. Hénin, W. Jiang, R. McGreevy, M. C. Melo, B. K. Radak, R. D. Skeel, A. Singharoy, Y. Wang, B. Roux, A. Aksimentiev, Z. Luthey-Schulten, L. V. Kalé, K. Schulten, C. Chipot and E. Tajkhorshid, *J. Chem. Phys.*, 2020, **153**, 044130.
65 J. Huang and A. D. Mackerell, *J. Comput. Chem.*, 2013, **34**, 2135–2145.